Challenge Journal of CONCRETE RESEARCH LETTERS

Vol.8 No.2 (2017)

CFRP acidic environment acoustic emission compressive strength concrete corrosion cracking ductility durability ferrocement fly ash mechanical properties palm oil fuel ash reinforced concrete self-compacting concrete silica fume steel mesh strength strengthening superplasticizer water a[illegible]ion

ISSN 2548-0928

TULPAR ACADEMIC PUBLISHING

Challenge Journal of Concrete Research Letters

E-mail: *cjcrl@challengejournal.com*

Web page: *cjcrl.challengejournal.com*

TULPAR Academic Publishing
www.tulparpublishing.com

Challenge Journal of Concrete Research Letters

CONTENTS

TULPAR ACADEMIC PUBLISHING

Challenge Journal of Concrete Research Letters

Effectiveness of high performance mortar reinforced with fibers as a repair material

Eethar Thanon Dawood *, Tamara Waleed Ganim

Department of Building and Construction Engineering, Technical College of Mosul, Northern Technical University, Mosul, Iraq

ABSTRACT

The present work deals with engineering properties of high performance mortar (HPM) to be used as a repair material. The experimental study was conducted on HPM reinforced with mono steel fibers and hybrid fibers consist of steel and polypropylene fibers. The economical efficiency of the designed mono and hybrid fibers reinforced mortar were presented. The results indicate that the hybridization of 1.8% steel fibers and 0.2% polypropylene fibers is very beneficial to decrease the production cost of fiber reinforced mortar for large scale construction project applications. The combined system of substrate concrete with different mixes of HPM was used to study its bond strength properties. The experimental tests are: two-part bond strength tests in additional to three part-bond strength tests. It was found that HPM reinforced by hybrid fibers has the best performance when two-part bond strength is required. On the other hand, in three parts bonding, the combined system of NC with epoxy has the best bond strength while HPM reinforced fibers show a better failure mode.

ARTICLE INFO

Article history:
Received 19 May 2016
Revised 16 April 2017
Accepted 15 May 2017

Keywords:
High performance mortar
Hybrid fibers
Economical benefits
Repair materials
TOPSIS

1. Introduction

Increasing service loads, excessive loading events, and exposure to an ever-changing ambient environment are some reasons why civil structures, over the service periods, degrade and ultimately develop performance deficiencies due to Haber et al. (2012). In several cases, it is economically more possible to repair and rehabilitate the structure than full destruction and reconstruction. Traditional methods of strengthening may include steel plating, addition of concrete, and near surface mounting additional steel. However, these methods have been proven valuable; but they can be cumbersome, time inefficient, and susceptible to corrosion due to Haber et al. (2012).

Recently different repair methods and materials are used to overcome damaged structures. The choice of them is a function of both the physico-chemical and the mechanical properties of the substrate based on Mallat et al (2011). A good repair material may improve the function and performance of the concrete structure. On the other hand, poor repair fails early or deteriorates the adjoining sound concrete material in a relatively short time as reported by Pattnaik (2006).

The repair materials should be contributed to the mechanical strength of the concrete structure and a high fluidity is required to fill cracks and pores completely. Besides, a repair material is sensitive to minor displacements and must have an elastic modulus as close as possible to that of the concrete substrate. Hence, a repair material with a high fluidity and a relatively high compressive strength is required due to Liu and Huang (2008).

Cemenititious composite are assumed to be highly compatible with concrete structure in terms of physical, chemical and mechanical properties in order to assure the long term durability as stated by Schueremans et al. (2011). Cementitious composites are typically characterized as brittle, with a low tensile strength and strain capacity. Fibers are incorporated into cementitious matrices to overcome this weakness, producing materials with increased tensile strength, ductility and toughness

* *Corresponding author*. Tel.: +964-770-1761858 ; E-mail address: eethar2005@yahoo.com (E. T. Dawood)
ISSN: 2548-0928 / DOI: https://doi.org/10.20528/cjcrl.2017.02.001

with improved durability due to Balaguru and Shah (1992). The character and performance of fiber-reinforced composites (FRC) change, depending on the properties of cementitious composites and the fibers according to Mehta and Monteiro (2006), and Kuder and Shah (2010).

The use of a single type of fiber may enhance the properties of FRC to a limited level. However, the concept of hybridization, which is the process of adding two or more types of fiber into concrete, can offer more attractive engineering properties. This is related to the presence of one fiber enables the more efficient utilization of the potential properties of the other fiber as reported by Sahmaran et al. (2005). Hybrid fibers of different sizes and types may play vital roles in resisting cracking at different scales, and consequently to achieve high performance. It has been proven that the incorporation of fiber into cementitious materials can significantly improve their toughness and ability of resisting crack, and many research works have been carried out on fiber-reinforced cementitious composites due to previous researches prepared by Mehta and Monteiro (2006), Kuder and Shah (2010), Sahmaran et al. (2005) and Sun et al. (2001).

Steel fiber has a considerably larger length and higher Young's modulus as compared to the other fiber-types due to Bentur and Mindes (1990). However, the addition of steel fibers at higher dosages has some disadvantages in terms of poor workability and higher cost. In addition, the high stiffness of steel fibers in the matrix means that voids and honeycombs could be formed during placing as a result of improper compaction at low workability as reported by Yao et al. (2003). The addition of flexible fibers (such as polypropylene fibers) leads to good fresh mortar properties and a reduction in early age cracking. The beneficial effects of flexible fibers can be attributed to their high aspect ratios and increased fiber availability (because of their lower density compared to steel) at a given volume fraction. Having lower stiffness, these fibers are particularly effective in controlling the propagation of microcracks in the plastic stage of concrete and their contribution to post-cracking behaviour is known to be significant according to significant studies prepared by Sahmaran et al. (2005), Sivakumar and Santhanam (2007) and Dawood and Ramli (2010).

Therefore, the objectives of this study are to produce high performance mortar reinforced with hybrid fibers and then tested for mechanical tests. Besides, the economic efficiency using TOPSIS is considered for such evaluation. Furthermore, the repair tests are prepared for the evaluation of such HPM.

2. Materials and Mix Proportions

2.1. Material properties

Ordinary Portland cement type I, was used in different mortar mixes. Metakaolin used in this study was subject to a thermal treatment at 750°C for 60 minutes. The chemical compositions of ordinary Portland cement and metakaolin are shown in Table 1. Superplasticizer has been provided by Sika ViscoCrete-SF 18 and was used to establish the desired workability of mixes. The fine aggregate was natural sand, with fineness modulus of 2.18. The steel fiber was low carbon cold drawn steel wire and their characteristic are shown in Table 2. The polypropylene fiber was supplied by AYLA Company and their characteristics are shown in Table 3. Epoxy was used in this study as a repair material for the damaged concrete. This material was produced by KÖSTER KB Fix.

Table 1. Chemical composition of ordinary portland cement.

Metakaolin % by weight	Ordinary Portland Cement % by weight	Constituent
1.39	62.20	Lime (CaO)
54.62	21.31	Silica (SiO_2)
41.06	5.89	Alumina (Al_2O_3)
1.60	3.62	Magnesia (MgO)
1.06	2.67	Iron oxide (Fe_2O_3)
0.1	2.60	Sulfur trioxide (SO_3)
6.12	1.59	Loss of ignition
-	33.37	C_3S
-	35.92	C_2S
-	11.09	C_3A
-	8.12	C_4AF

Table 2. Characterization of steel fibers.

Fiber properties	Quantity
Average fiber length (mm)	12
Average fiber diameter (mm)	0.20
Aspect ratio (l/d)	60
Tensile strength (MPa)	>1100
Ultimate elongation (%)	4
Specific gravity	7.85

Table 3. Characterization of polypropylene fibers.

Fiber properties	Quantity
Average fiber length (mm)	12
Tensile strength (MPa)	137-689
Young's Modulus (GPa)	3.4-4.8
Toughness (GPa)	8.82
Elongation (%)	25-40
Specific gravity	0.9
Melting point (°C)	160

2.2. Mix proportions

The mortar compositions are given in Table 4. A total of eleven mortar mixes were prepared using water-binder (cement + metakaolin) in a ratio of 0.40 and the metakaolin was used in the porder of 10% as a partial

replacement of cement. The amount of cement, metakaolin, sand and free water were kept constant. The amount of superplasticizer varied from 1.5% to 2.2% by weight of binder content to maintain flowability for all the mixes. The steel fibers were added to the mix according to the volumetric fraction of 1.0, 1.2, 1.4, 1.6, 1.8 and 2.0% of the mixes was used in preparing the M1-M6 mixes. However, the 2% hybrid mix of fibers was composed of different amounts of steel and polypropylene fibers in the preparation of mixes M7 to M10.

Table 4. High performance mortar mix proportions.

Index	Cement (kg/m³)	MK (kg/m³)	Sand (kg/m³)	SP (%)	W/C	SF (%)	PPF (%)	Flow (%)
M0	585	65	1462	1.5	0.4	-	-	130
M1	585	65	1462	1.5	0.4	1.0	-	130
M2	585	65	1462	1.5	0.4	1.2	-	130
M3	585	65	1462	1.5	0.4	1.4	-	125
M4	585	65	1462	1.5	0.4	1.6	-	125
M5	585	65	1462	1.8	0.4	1.8	-	120
M6	585	65	1462	1.8	0.4	2.0	-	120
M7	585	65	1462	2.0	0.4	1.8	0.2	120
M8	585	65	1462	2.0	0.4	1.6	0.4	115
M9	585	65	1462	2.2	0.4	1.4	0.6	110
M10	585	65	1462	2.2	0.4	1.2	0.8	100

2.3. Test methods

Three cube 50×50×50 mm samples were used for each mix to test the compressive strength at various ages 7, 28 and 90 days according to ASTM C109. The flow test for mixes was performed according to ASTM C230 with a designed flow of 130%. The cube specimens were left in the molds for 24 hours at 20 °C after casting. After demolding, the specimens were kept in plain water until the time of the test. Compressive strength test was performed directly after the density test according to ASTM C642. Splitting tensile test was achieved using 150 × 300 mm cylinders according to ASTM C469. Bond strength test (slant shear) was tested using cylinder 76.2×152.4 mm according to ASTM C882. Besides, three 40×40×160 mm prismatic steel molds were used to prepare the specimens for the flexural strength test according to ASTM C348, and the toughness indices were determined according to ASTM C1018.

2.3.1. Two-Part bond strength tests

The design of normal concrete used as substrate, are given in Table 5. The normal concrete is proposed here as substrate concretes that it needs to be repaired using repair materials. NC substrate are cast at 28-day earlier than the repair material and the composite specimens were tested after curing period of 28-day. The specimens of that concrete were sawed and the interface surface prepared by sandblasting to connected by repair materials in one system. Also the failure modes were examined for all test specimens.

Table 5. Mix proportions of normal concrete used as substrate concrete.

Mix	W/C	Cement (kg/m³)	Sand (kg/m³)	Gravel (kg/m³)	M.A.S (mm)	Slump (mm)
NC substrate	0.5	320	640	1280	10	50

In the test of slant shear strength, the repair mortar is bonded to a substrate concrete specimen on a slant elliptical plane inclined at 30° angle from vertical to form a 75×150 mm composite cylinder as shown in Fig. 1. Before the repair mortar is bonded, the slant surface of the substrate concrete specimen is prepared by sandblasting as shown in Fig. 2(a).

The change in the water/binder ratio of the fresh repair mortar due to the water absorption of pre-cast NC halves might result in a decrease in its workability. Hence, all halves cylindrical specimens were cured in water for an additional 24 h before repair mortar was poured. The test is performed by determining the compressive load required to fail the composite cylinder and the bond strength is calculated as [*max load*] / [*area of elliptical surface*].

In the test of splitting tensile strength, the composite specimen was constructed with one-half substrate concrete and other-half repair mortar as shown in Fig. 3. The interface surface of the substrate concrete specimen is prepared by sandblasting Fig. 2(b). The test is performed by determining the split tensile load required to fail the composite cylinder and the bond strength is calculated as [*max load*] / [*area of half cylinder*].

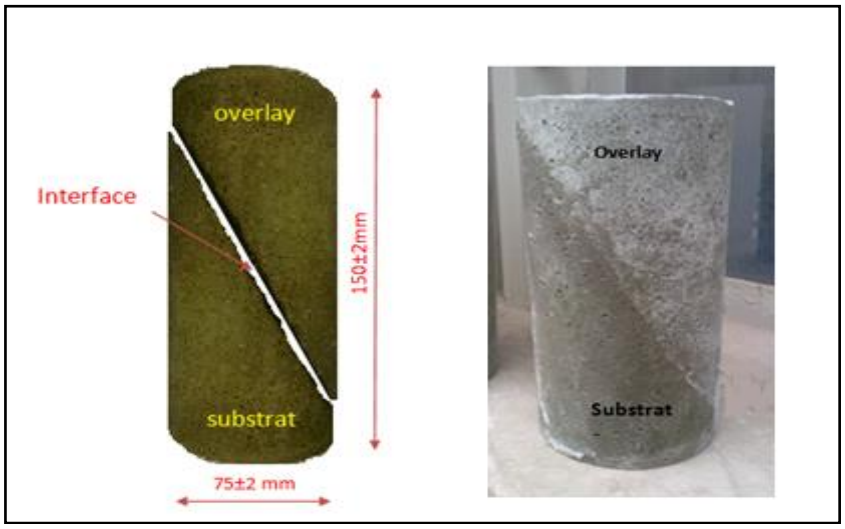

Fig. 1. Composite specimen for slant shear bond strength test.

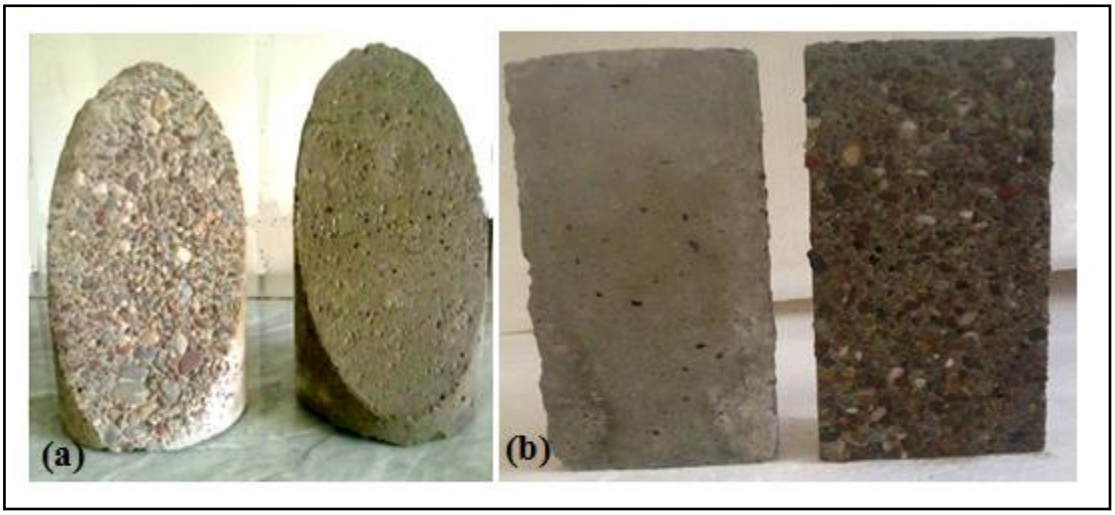

Fig. 2. Preparation of interface substrate concrete by sandblast.

Fig. 3. Composite specimen for splitting tensile strength.

2.3.2. Three-Part bond strength tests

In the test of slant shear, bond strength of the repair materials is determined using ASTM C882 as shown in Fig. 4. In this test procedure, a fresh mortar/epoxy layer with a thickness of 20 mm was placed on the diagonal bonding area between the two halves of NC substrate. Before the repair materials are bonded, the slant surface of the substrate concrete specimen is prepared by sand-blasting. At the same time, the interface surface prepared by dry brushing for epoxy bonding. The bond strength is calculated as [*max load*] / [*area of elliptical surface* × 2].

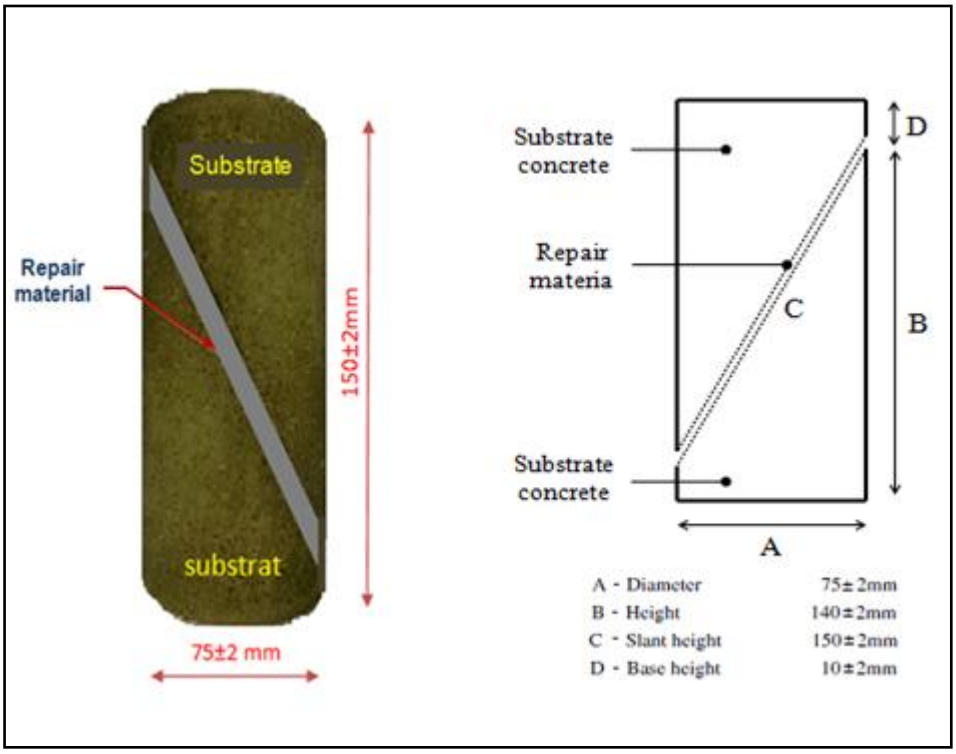

Fig. 4. Composite specimen for slant shear bond-strength test (three-part).

In the flexural strength test, concrete prisms 100×100×400 mm was cast as per standard ASTM C78 test procedure. The specimens of that concrete were sawed and the interface surface prepared by sandblasting shown in Fig. 5. The composite prism of repair material with substrates concrete was fabricated to the same dimensions as the control prism, with the exception that combining two substrate concrete portions by 20 mm mortar/epoxy materials at 45° as show in Fig. 6.

3. Test Results and Discussion

3.1. Pozzolanic activity index

The mean values of PAI for HPM replaced by 0, 5, 10 and 15% of MK after 7 and 28 days is obtained in Fig. 7. This figure indicates clearly that the highest compressive strength was obtained using 10% of total cementitious materials. This percentage of the metakaolin as a partial replacement of cement increases the compressive strength of the cement-mortar owing to the pozzolanic reaction between the amorphous silica in metakaolin and calcium hydroxide produced by the hydration of Portland cement due to Ramezanianpour and Jovein (2012). The use of more than 10% of metakaolin lessens the improvement in compressive strength and this may be due to the fact that C–S–H produced by metakaolin has a lower C: S ratio than the C–S–H resulting from the hydration of Portland cement alone as stated by the study prepared by Mustafa and Yaman (2007).

Fig. 5. Sandblast the two halves of NC substrate.

3.2. Flowability

Table 6 listed the flowability of HPM mixes reinforced with fibers. The inclusion of the fibers in HPM mixes reduces the flowability as fibers volume fraction increased due to Izaguirre et al. (2011). Thus; increasing the amounts of superplasticizer was needed to achieve the desired level of workability and to get a proper distribution of the fibers. The inclusion of 2% individual steel fiber "M6" reduced the value of the flow from 130 mm to 120 mm, despite increasing in SP dosage from 1.5% to 1.8%.

On the other hand, increasing of SP dosage up to 2.2% in the hybrid mix of 1.2% steel fiber plus 0.8% polypropylene fiber "M10", also conduct a reduction in flowability up to 100 mm. Therefore, it can be stated that individual steel fibers showed lesser effect on the flow capacity than that of steel plus polypropylene hybrid fibers relate to the inclusion of polypropylene fibers as reported by Bendjillalia et al. (2011).

Fig. 6. Composite prism of substrates concrete.

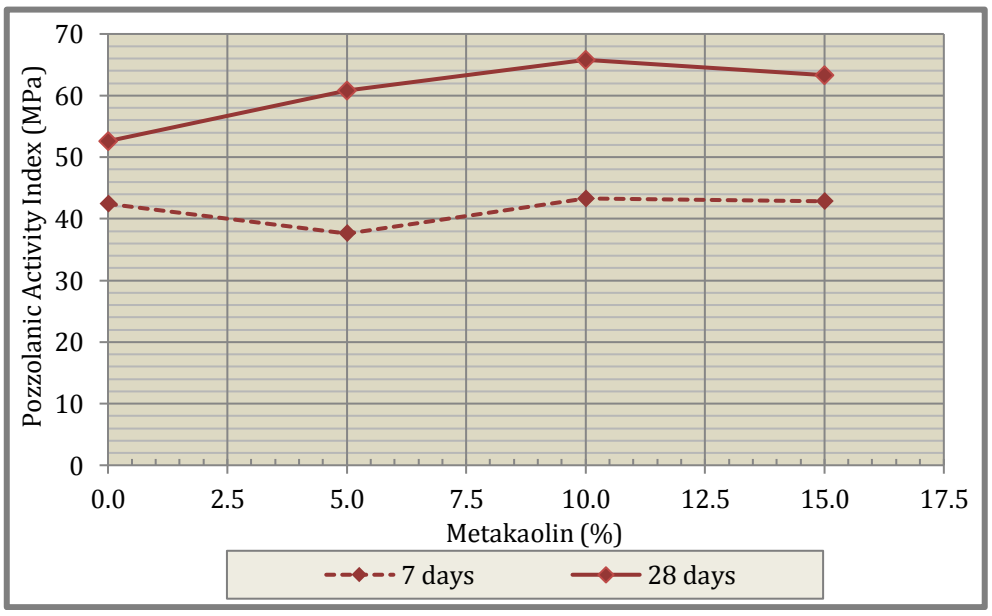

Fig. 7. Relationship between metakaolin percentage and PAI for HPM mixes.

Table 6. Flow of HPM mixes.

Index	M0	M1	M2	M3	M4	M5	M6	M7	M8	M9	M10
SP (%)	1.5	1.5	1.5	1.5	1.5	1.8	1.8	2.0	2.0	2.2	2.2
Flow (%)	130	130	130	125	125	120	120	120	115	110	100

3.3. Compressive strength

The results in Fig. 8 show the compressive strength of HPM mixes at 7 to 90 days. For HPM reinforced with different percentages of mono steel fibers (1, 1.2, 1.4, 1.6, 1.8 and 2%) as a volume fraction, the results in Table 7 indicate that the compressive strength increases with fibers content increase.

This enhancement in the compressive strength is most likely due to the fact of a reduction in the porosity of HPM and an enhancement in the mechanical bond strength due to Miloud (2005). These results are comparable with other researches in this regard who are Mohammadi et al. (2005). The increase in compressive strength of HPM incorporating with 2% steel fiber "M6" at 28-day was up to 14% compared to the reference mix "M0". This enhancement in the compressive strength may have resulted from the short length, high stiffness and high modulus of the steel fibers used in this study. As well as the ability of steel fiber to eliminate the microcrack of the cementitious matrix due to Steffen and Joost (2001) and Mustafa and Yaman (2007). The effect of steel fibers percentage on compressive strength of HPM is showed in Fig. 9.

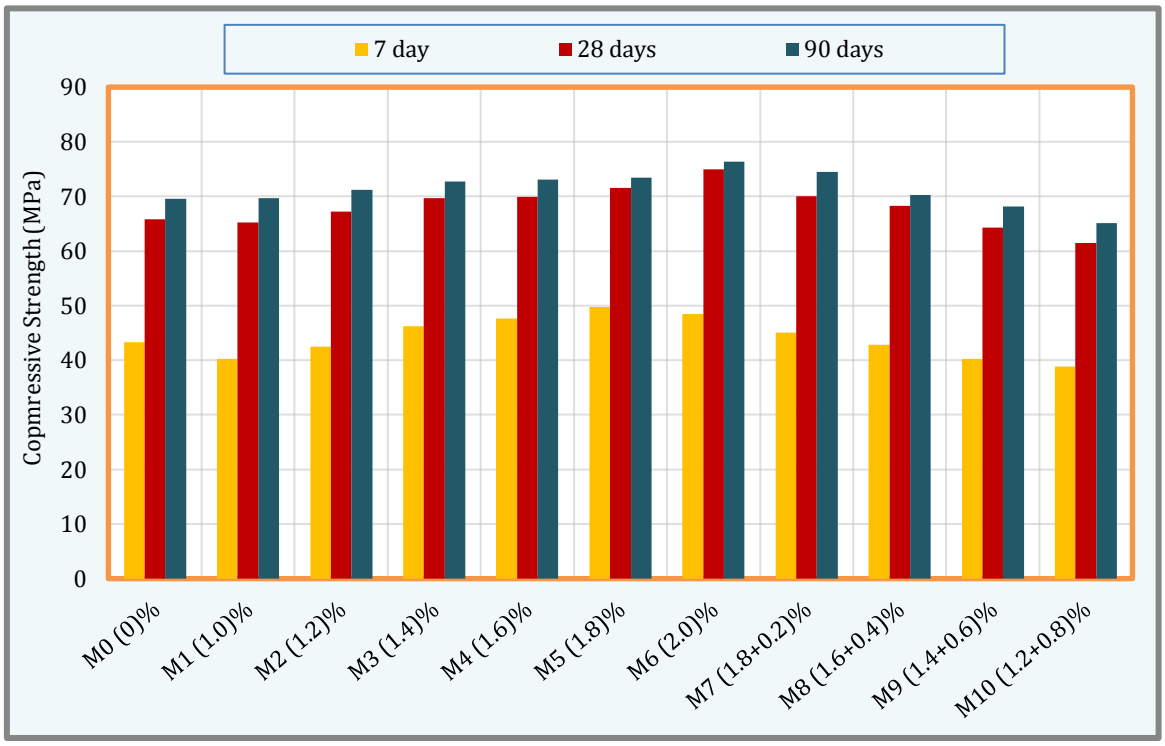

Fig. 8. Compressive strength of HPM reinforced different percentage of mono and hybrid fibers at different ages.

Table 7. Mechanical properties of HPM mixes.

Index	Steel fiber (%)	Polypro-pylene fibers (%)	Compressive strength (MPa) 7-day	Compressive strength (MPa) 28-day	Compressive strength (MPa) 90-day	Splitting tensile strength (MPa) 28-day	Flexural strength (MPa) 28-day
M0	-	-	43.30	65.80	69.50	3.10	9.14
M1	1.0	-	40.30	65.20	69.70	3.14	9.38
M2	1.2	-	42.50	67.20	71.20	3.16	9.27
M3	1.4	-	46.20	69.70	72.20	3.26	9.70
M4	1.6	-	47.60	69.90	73.10	3.45	9.75
M5	1.8	-	49.70	71.60	73.40	3.50	10.08
M6	2.0	-	48.50	74.90	76.30	3.65	10.50
M7	1.8	0.2	45.10	70.00	74.50	3.52	10.17
M8	1.6	0.4	42.80	68.30	70.30	3.35	10.10
M9	1.4	0.6	40.20	64.30	68.10	3.30	9.54
M10	1.2	0.8	38.80	61.50	65.10	2.90	8.86

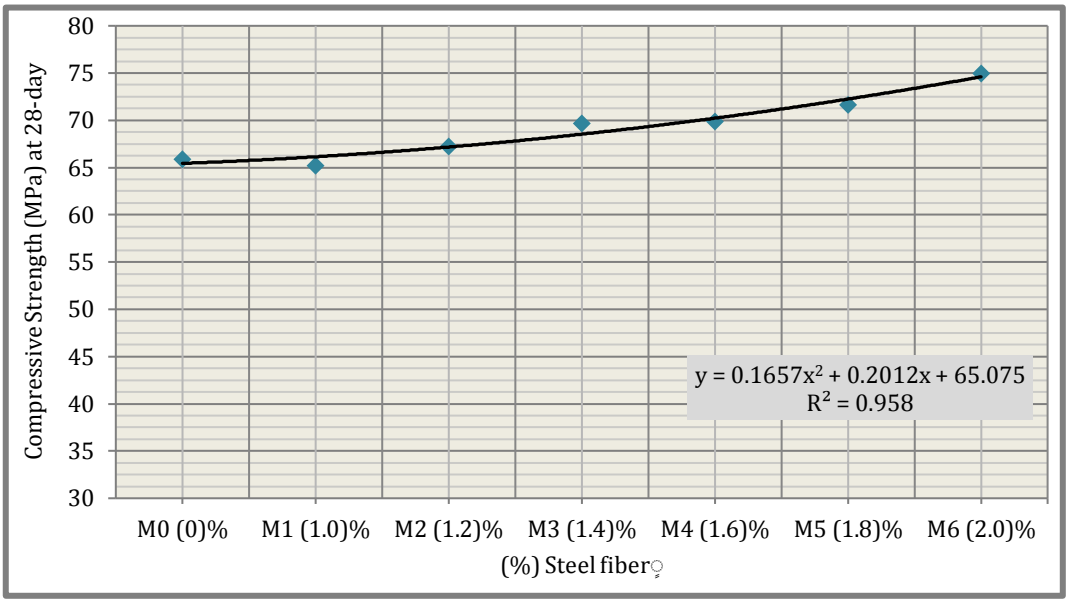

Fig. 9. Relationship between steel fibers content with compressive strength of HPM mixes.

On the other hand, for HPM reinforced with steel and polypropylene hybrid fiber, the comparison between reference mix "M0" with 1.8% steel fiber + 0.2% polypropylene fibers "M7" shows that this hybridization increase the compressive strength by about 7%. Furthermore, the use of 1.6% steel fiber + 0.4% polypropylene fibers "M8" shows increase in compressive strength by about 4%. On the other hand, the inclusions of 1.4% steel fiber + 0.6% polypropylene fibers "M9" and 1.2% steel fiber + 0.8% polypropylene fibers "M10" decrease the compressive strength of HPM by about 2.4% and 6.6%, respectively. This can be attributed to the low stiffness and also the ductility of the polypropylene fibers compared by steel fiber, as well as non-homogeneous distribution of polypropylene fibers generating a coherent matrix due to Markovic (2003). These observation is also supported by Qureshi et al. (2013) that also observed from their results that the increase of polypropylene fibers replacement shows a reduction in compressive strength, they showed the hybridization of (60 kg/m^3 SF% + 1.5 kg/m^3 PPF) decrease the compressive strength up to 13%. In the summary, the effects of steel-polypropylene hybrid fibers on the compressive strength depended on the percentage of steel fibers replaced by polypropylene fibers. The effect of hybrid fibers on compressive strength of HPM is illustrated in Fig. 10.

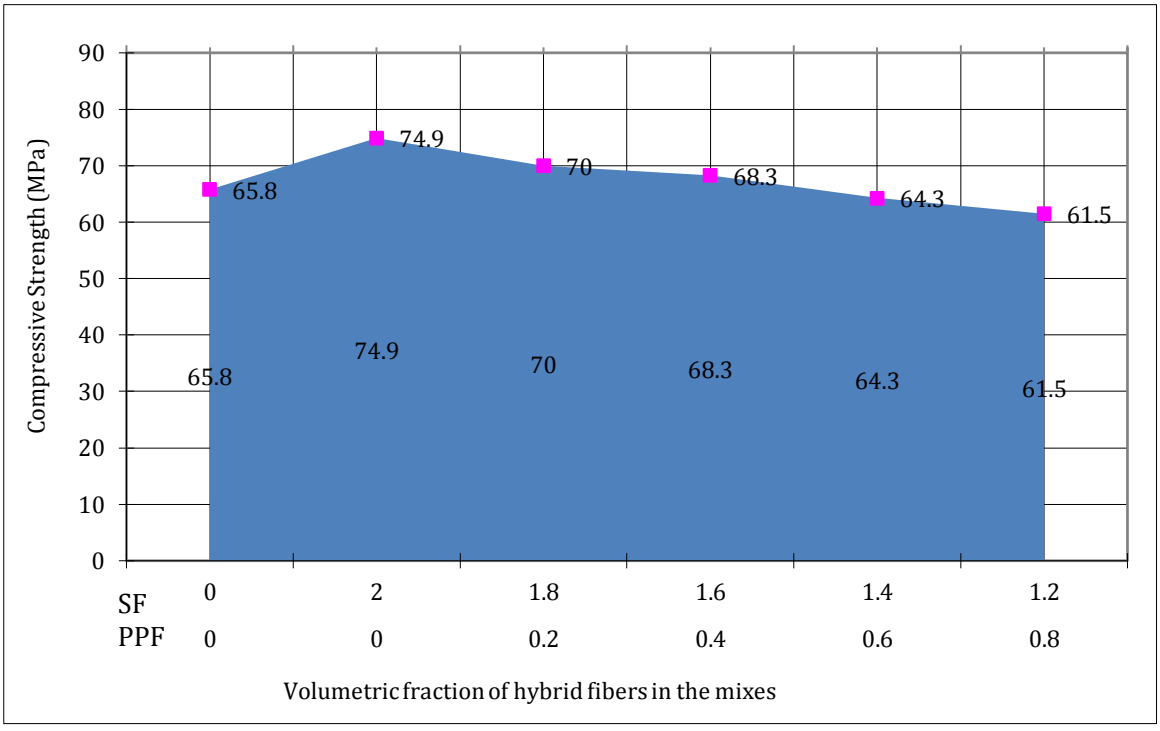

Fig. 10. Relationship between hybrid fibers content (steel+polypropylene) with compressive strength of HPM mixes.

3.4. Splitting tensile strength

For HPM reinforced with steel fibers, the splitting tensile strength increased with an increase of steel fibers content as show in Table 7. HPM reinforced with 2.0% steel fiber as a volume fraction has splitting tensile strength higher than control mix at 28-day by about 18%. This increment may attribute to the high tensile strength of the fibers which bridge the cracks and enhance the splitting tensile of HPM as also supported by other researchers; Aydin (2007), and Dawood and Ramli (2012). The relationship between steel fibers content with splitting tensile strength of HPM mixes are shown in Fig. 11.

On the other hand, for HPM reinforced with steel and polypropylene hybrid fibers, the splitting tensile strength of the HPM at 28 days was up to 13.5% for mortar mix reinforced with 1.8% steel fibers + 0.2% polypropylene fibers "M7" compared with the reference mix "M0". The splitting tensile strength increased by about 8.0% and 6.5% for mixes with 1.6% steel fibers + 0.4% polypropylene fiber "M8" and 1.4% steel fibers + 0.6% polypropylene "M9", respectively. The hybridization of 1.2% steel fibers + 0.8% polypropylene fiber "M10" shows a decrease in splitting tensile strength by about 6.8%. The effect of hybrid fibers content on splitting tensile strength of HPM is illustrated in Fig. 12.

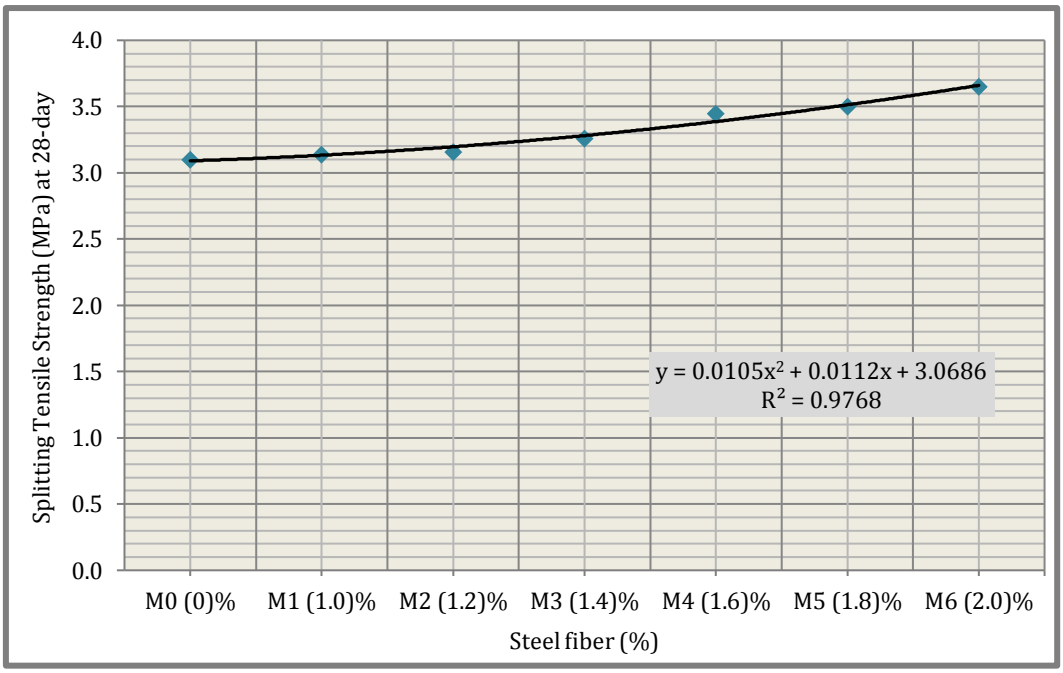

Fig. 11. Relationship between steel fibers content with splitting tensile strength of HPM mixes.

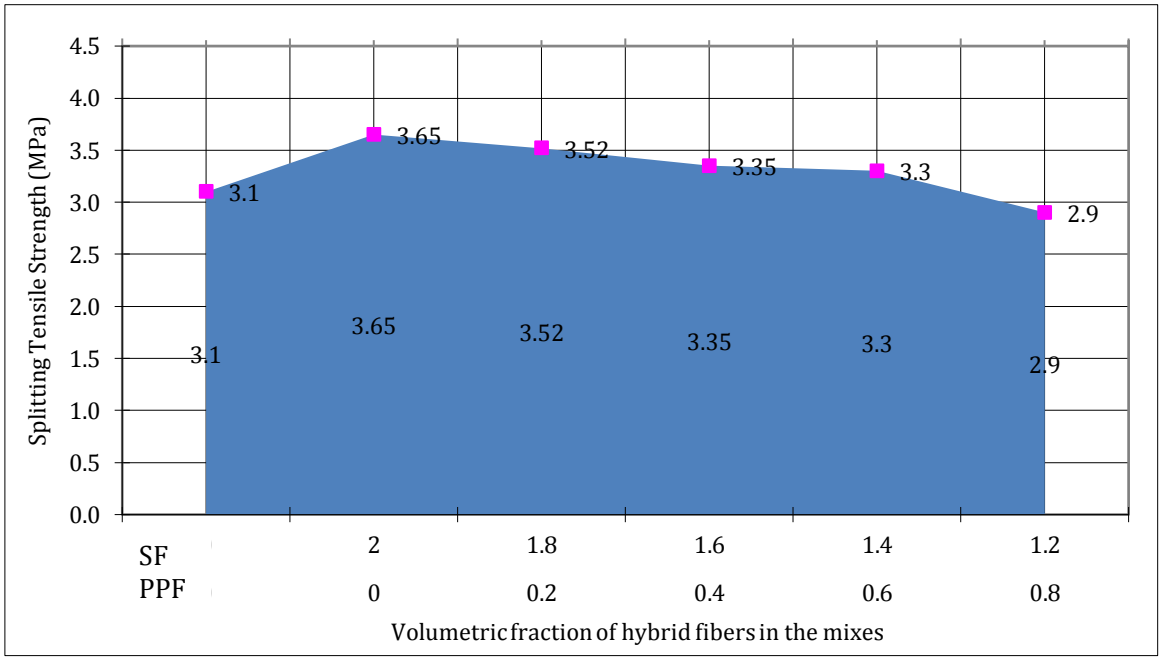

Fig. 12. Relationship between hybrid fibers (steel+polypropylene) with splitting tensile strength of HPM mixes.

As a result it can be stated that the effect of hybrid fiber in splitting tensile strength is expected since the plane of the failure is well defined diametric 'splitting'. The higher the number of fibers is bridging the diametric crack, the higher would be the split tensile strength due to Sivakumar and Santhanam (2007). However, fiber availability is not the only parameter governing the strength; the stiffness of the fiber is also a major parameter affecting the strength. The increased fiber availability of polypropylene fiber with the high stiffness of steel fiber resulted in a significant enhancement of the split tensile strength for these combinations up to a specific limit.

3.5. Flexural tensile strength

The results of flexural strength of HPM are illustrate in Table 7. For HPM mixes reinforced with individual steel fiber, flexural strength demonstrated an appreciable increase in flexural strength with a percentage increase of steel fibers. HPM mix containing steel fiber up to 2% "M6" has a flexural strength up to 15% higher than that of the control mix "M0". It was observed that, the formations of cracks were extended in the specimens without steel fibers "reference mix" in greater numbers. Whereas, they were the least in the specimens reinforced with the highest steel fibers content used in this study such observation are comparable by other researches in this regard; Dawood and Ramli (2010) and Koksal et al. (2008) .The effect of steel fibers percentage on flexural strength of HPM is illustrated in Fig. 13.

As a result, the increase in flexural strength, increase the resistance against crack propagation due to the loads effects and decrease the possible crack propagation due to internal stresses occurring in the matrix, since the use of steel fibers makes mortar stronger and thus durable against the cracks due to Mohammadi et al. (2005), and Sevil et al. (2011).

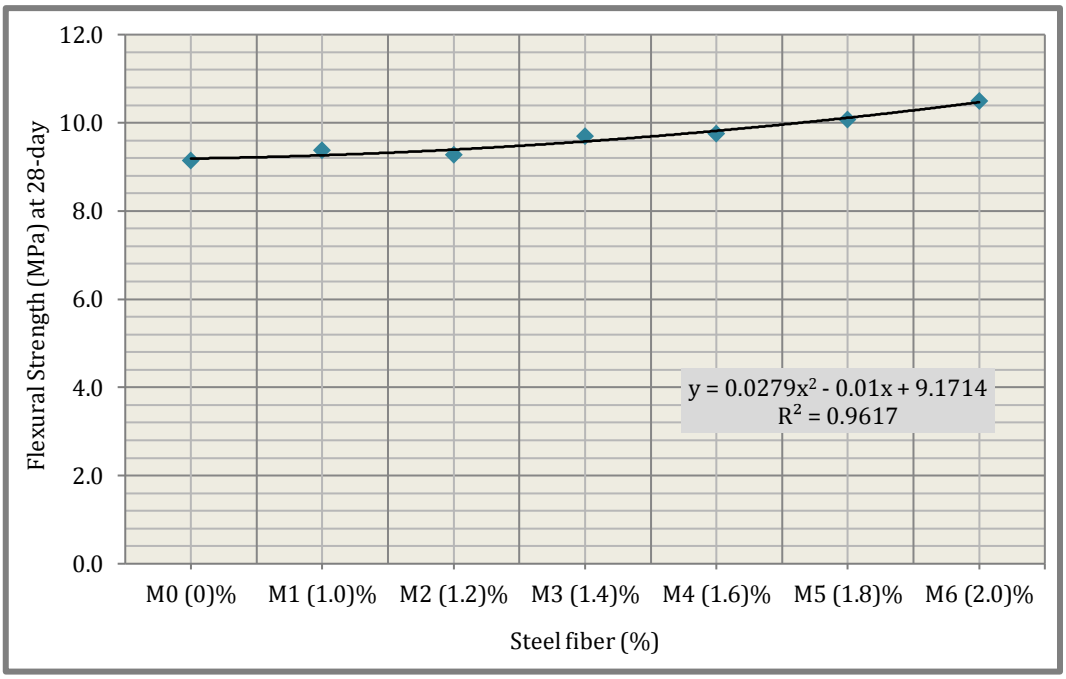

Fig. 13. Relationship between steel fibers content with flexural strength of HPM mixes.

On the other hand, for HPM mix reinforced with hybrid fiber, the hybridization of two fiber types and the aspect ratio showed noticeable enhancement in peak load as supported by other researchers; Hsie et al. (2008). The use of 1.8% steel fiber + 0.2% polypropylene hybrid fibers "M7" increased the flexural strength of HPM at 28 days by about 11.3% compared with the reference mix "M0". In addition, the flexural strength increased by 10.5% and 4.4% for M8 and M9 respectively, then the flexural strength decrease at hybridization of 1.2% steel fiber + 0.8% polypropylene fibers mix "M10" by about 3%.The effect of hybrid fibers content on flexural strength of HPM is illustrated in Fig. 14. It can be stated that the flexural strength of hybridization fibers mixes depends on the volume fraction of steel fiber, related to the high stiffness as compared to polypropylene fiber due to Campello et al. (2014). The latter fibers are more efficient in delaying the growth and propagation of micro- and meso-cracks before peak load due to Qureshia et al. (2013). Whereas polypropylene fiber at high content level led to an obvious decrease in strength, likely due to poor dispersion and agglomeration of the fibers in the matrix as also supported by Bendjillalia et al. (2011).

3.6. Flexural toughness

The results of flexural toughness at 28 days were evaluated using the ASTM C1018 test method. The toughness indices results of HPM mixes with different percentages of individual and hybrid fiber are discussed in this section. In essence, toughness is defined as the ability of fiber reinforced concrete to absorb energy before failure due to its post cracking performance, where the included fibers serves to prevent concrete failure and separation

due to Natali et al. (2011). The toughness indices I5, I10 and I30 for different mixes in three-point bending are given in Table 8. For an elastic-brittle material, all indices should be 1. But for an elastic-ideal plastic material, I5, I10 and I30 should be closer to 5, 10 and 30, respectively due to Balendran et al. (2002). Fig. 15 shows toughness indices of HPM mixes, for the reference mix (without fibers) toughness indices is taken equal to 1.0 because the reference mix specimens in flexural test fail immediately after formation of the first crack.

For perusal of the result, HPM mixes reinforced with individual steel fibers, there is evident that the indices I5, I10 and I30 increase with increasing of fiber content in HPM mix. It can be clearly observed that the indices I30 are relatively higher susceptibility to the fiber content compared with I5 and I10 indices. This observation can be attributed based on the stiffness property and the mechanical performance of steel fibers which make them more efficient in this stage according to Lawler et al. (2003). However, the use of 2% of steel fiber boosts the toughness indices I5, I10 and I30 at 28-day by about 4.52, 8.46 and 19.0, respectively.

This enhancement can be attributed to the ability of steel fibers in the arresting cracks at both micro-and macro-levels. At the micro-level, fibers inhibit the initiation of cracks, while at the macro-level, fibers provide effective bridging and impart sources of toughness and ductility as supported by other researchers; Banthia and Sappakittipakorn (2007), and Dawood and Ramli (2011).

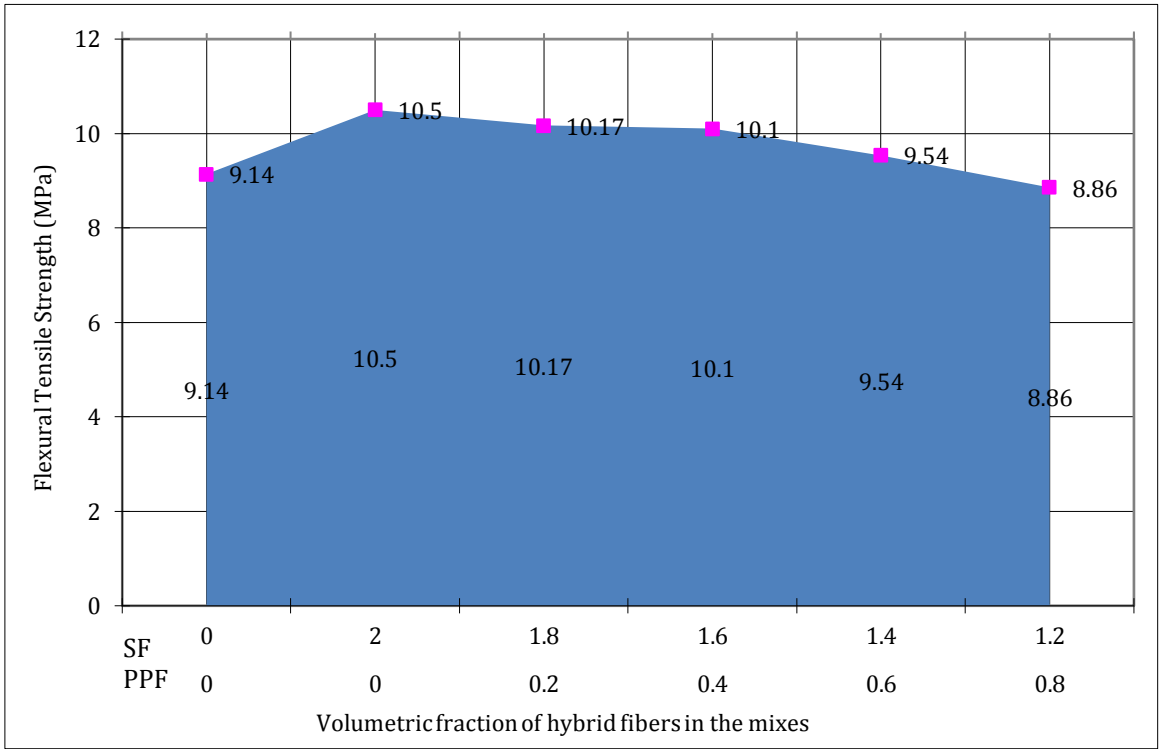

Fig. 14. Relationship between hybrid fibers content (steel+polypropylene) with Flexural strength of HPM mixes.

Table 8. Toughness indices of HPM mixes.

Index	Steel fiber (%)	Polypropylene fiber (%)	Toughness Indices I5 28-day	Toughness Indices I10 28-day	Toughness Indices I30 28-day
M0	–	–	1.00	1.00	1.00
M1	1.0	–	4.16	7.8	15.04
M2	1.2	–	4.44	8.15	15.59
M3	1.4	–	4.01	7.18	15.62
M4	1.6	–	4.46	8.43	17.59
M5	1.8	–	4.31	7.95	17.63
M6	2.0	–	4.52	8.46	19.00
M7	1.8	0.2	4.11	7.52	17.20
M8	1.6	0.4	4.83	8.80	16.65
M9	1.4	0.6	4.59	8.21	14.30
M10	1.2	0.8	4.53	7.69	9.72

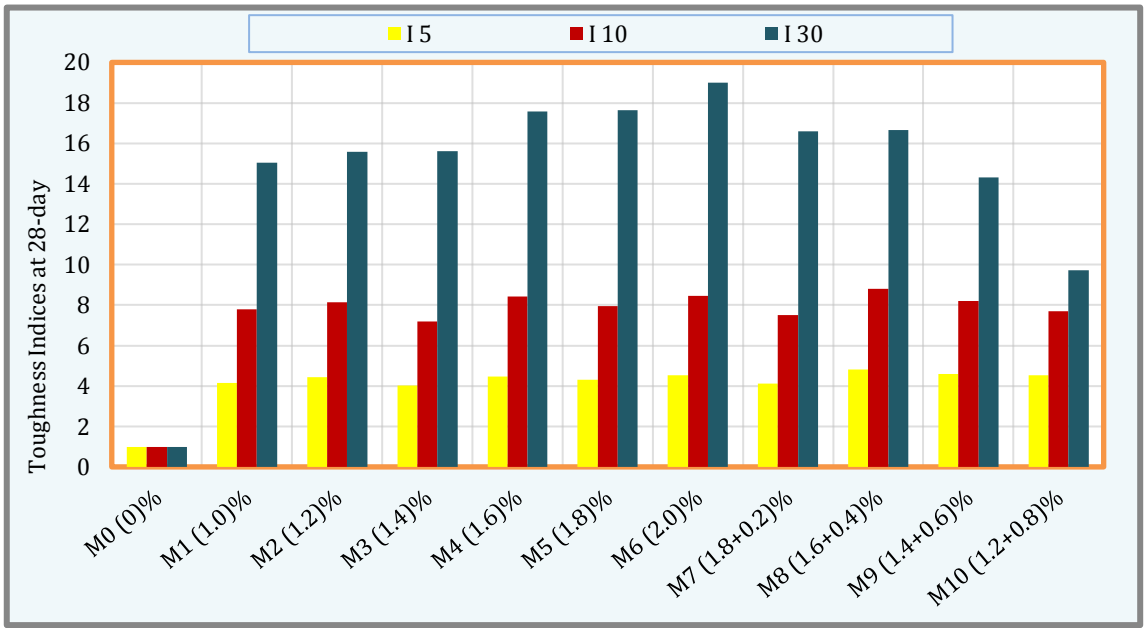

Fig. 15. Toughness indices of HPM mixes at 28-day.

Fig. 16 shows the load–deflection relationship of HPM containing individual steel fiber, it was clearly observed the linearly behave from start loading up to first crack. Then; the majority of additional of steel fiber volume fraction is localized at the crack after the peak load, where the drop in load are accurse. The noticed drops in load seem to be higher for mixes containing lower fiber content and smaller for mixes containing higher ones due to Abd ElAty (2013).

For HPM reinforced with steel and polypropylene hybridization fibers, the highest improvement of toughness indices was found at the combining of 1.8% steel fiber + 0.2% polypropylene fiber "M7" as shown in Table 8. However, flexural toughness indices I5, I10 and I30 of such mix were found as 4.11, 7.52 and 17.2, respectively. It was clearly noticeable that the indices I30 were decreased with the increase of partial replacement of steel fibers by non-metallic fiber (polypropylene fibers). This behavior is related to insufficient steel fiber in this system for bridging the wider cracks as supported by Sivakumar and Santhanam (2007). From the results, it is evident that the ductility of HPM reinforced fiber depends primarily on the fiber's ability to bridge the cracks at high level of strain. Thus, stiffer fibers would be providing better crack bridging; this explains the good performance of steel fiber compared to polypropylene fibers due to Campello et al. (2014).

The load–deflection relationship for steel and polypropylene hybrid fiber mixes is shown in Fig. 17. It was being noticed that the fracture tends to reduce the drop of the load values after the peak load and also with increasing in polypropylene fiber replacement. However the steel fibers have more effect on the post crack strength and the polypropylene fibers has more effect on first crack zone. This observation can be attributed to the fact that the steel fibers which are much stiffer than polypropylene in the hybrid fiber system provide reasonable first crack strength and ultimate strength, whereas polypropylene fibers are relatively flexible and lead to improved toughness and strain capacity in the post-crack zone due to Qureshi et al. (2013).

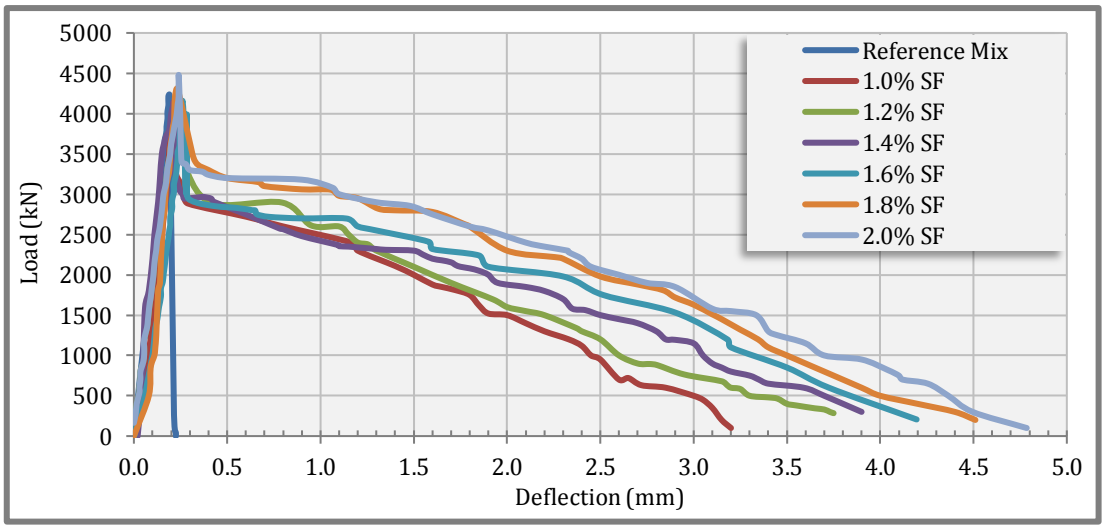

Fig. 16. Effect of steel fibers on flexural toughness of HPM mixes.

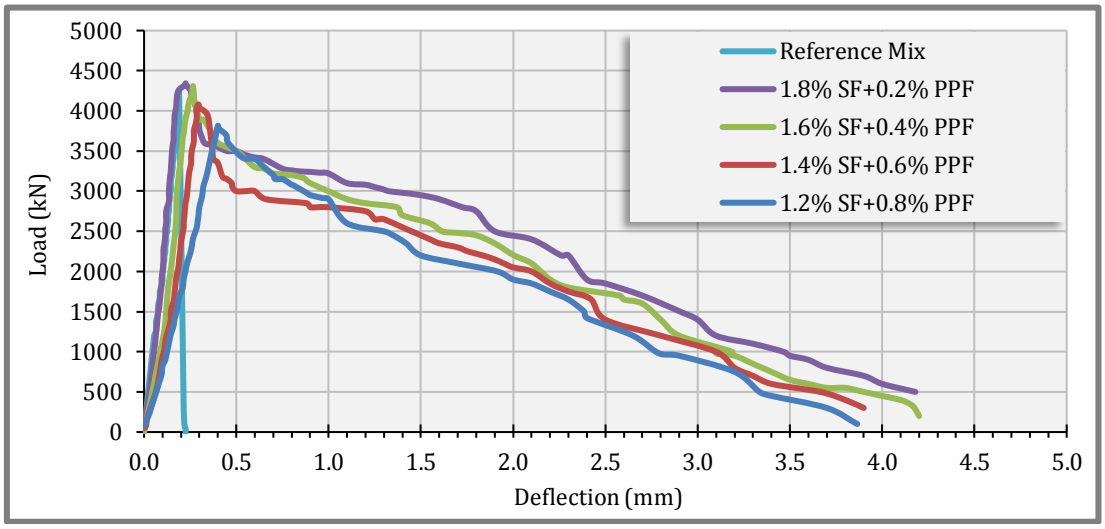

Fig. 17. Effect of hybrid fibers on flexural toughness of HPM mixes.

3.7. Bond strength

Slant shear test as per the specification of ASTM C882 was used to investigate the bond strength between NC substrate and HPM. The HPM was cast and bonded to the NC substrate specimens on a slant plane inclined angle of 30° from the vertical axis to form 75×150 mm composite cylinder specimens. The NC substrate specimens cast 28 days earlier than the overlay mortar, slant surface of the substrate concrete specimen was prepared by sandblasting. Where the interface was subjected to a combination of shear stress and compression forces, the slant shear test is the most appropriate test for such bond assessments.

The experimental results slant shear test presented in Fig. 18. Slant shear strength of composite cylindrical specimens of "M0" mix at 28-day was 10.5 MPa and this strength was increased with an increase of mono steel fiber reinforcement. This observation provided a means to the influence of the disparity of the mechanical properties of the HPM mixes due to Tayeha et al. (2013). The use of 2% volumetric fraction of steel fiber "M6" increased the slant shear strength by about 31% compared to reference mix "M0". On the hand, for HPM mixes reinforced with hybrid fibers, the HPM mix reinforced with 1.8% steel fibers + 0.2% polypropylene fiber mix "M7" exhibited the highest performance in this regard. Such increment was up to 58% compared with the reference mix. As well as bond strength was increased by about 39%, 25% and 14% for mixes M8, M9 and M10, respectively.

ACI Concrete Repair Guide as stated by Chynoweth et al. (1996) specifies the acceptable bond strength for repair work shall within the ranges of 13.8-20.7 MPa for slant shear strength at test ages of 28 days. This guideline is particularly useful for the selection of mortar mixes; M6, M7 and M8 to be used in a repair work.

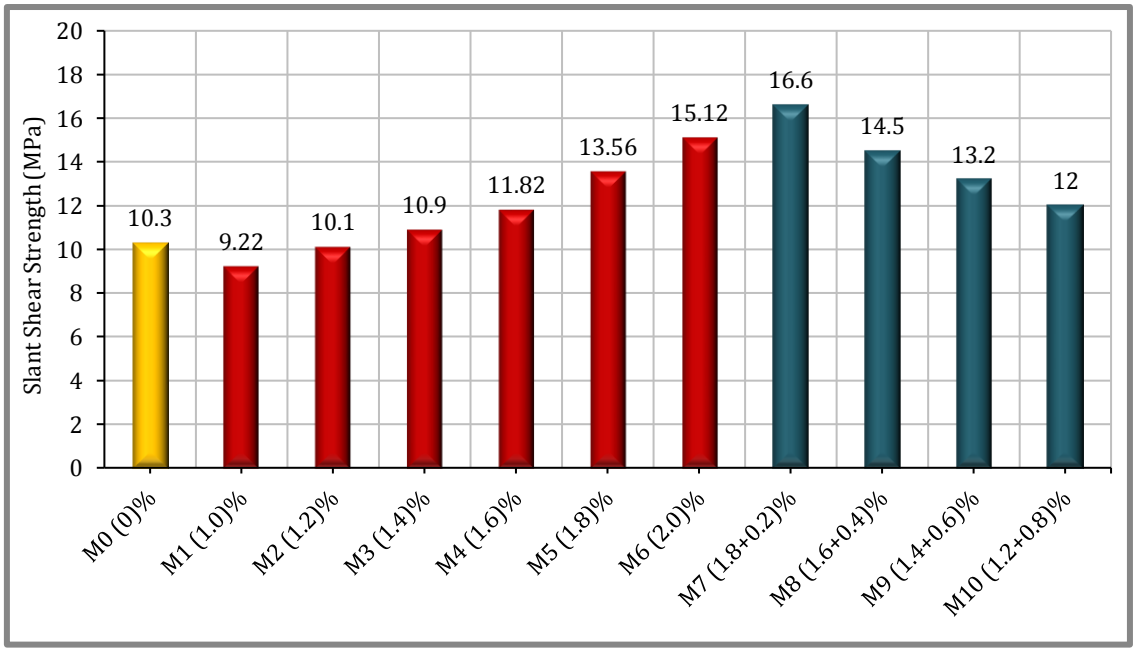

Fig. 18. Relationship between mono and hybrid fibers content with slant shear strength of HPM.

3.8. Dry density

The oven dry density of hardened HPM was determined according to ASTM C642. The results of the dry density test are listed in Table 9. The results at 28 days indicated that the use of steel fibers in HPM mixes increased the overall density of the mortar. The density value increased from 2170 kg/m^3 to 2230 kg/m^3 by the inclusion of 2% steel fibers. By contrast, it can be observed that increasing the amount of polypropylene replaced by steel fiber in the hybridization system reduced the density of the mortar. Therefore, the use of 0.8% of polypropylene fibers with 1.2% of steel fibers reduced the density to 2170 kg/m^3. As anticipated, the specific gravity of polypropylene fiber and the displacement of the mortar matrix during the mixing process reduce the density of the mixes as also supported by other study prepared by Momtazi and Zanoosh (2011).

Table 9. Dry density of HPM mixes.

Index	M0	M1	M2	M3	M4	M5	M6	M7	M8	M9	M10
Steel fiber (%)	–	1	1.2	1.4	1.6	1.8	2	1.8	1.6	1.4	1.2
Polypropylene fiber (%)	–	–	–	–	–	–	–	0,2	0.4	0.6	0.8
Dry Density (kg/m^3) (28-day)	2170	2170	2180	2190	2200	2220	2230	2215	2185	2180	2170

3.9. Economical efficiency

In order to give a clearer picture about the real benefits of using the designed mono and hybrid fibers, a classical method called TOPSIS (Technique for Order Performance by Similarity to Ideal Solution) is used to consider the compressive strength, flexural strength, toughness indices and bond strength in combination with the fiber cost as also adopted by other studies prepared by Hshiung and Jih-Jeng (2011) and, Tien-Chin and Tsung-Han (2007).

Table 10 illustrates the data of the reinforcement mixes with their mechanical properties and cost in I.D. used in this mathematical method.

Table 10. Properties of HPM mixes used in TOPSIS method.

Index	Steel fiber (%)	Polypro-pylene fiber (%)	Compressive strength (MPa)	Flextural strength (MPa)	Toughness indices I 30	Bond strength (MPa)	Cost
M1	1.0	–	65.20	9.38	15.04	9.22	785.00
M2	1.2	–	67.20	9.27	15.59	10.10	942.00
M3	1.4	–	69.70	9.70	15.62	10.90	1099.00
M4	1.6	–	69.90	9.75	17.59	11.82	1256.00
M5	1.8	–	71.60	10.08	17.63	13.10	1413.00
M6	2.0	–	74.90	10.50	19.00	13.80	1570.00
M7	1.8	0.2	70.00	10.17	17.20	16.61	1425.60
M8	1.6	0.4	68.30	10.10	16.65	14.50	1281.20
M9	1.4	0.6	64.30	9.54	14.30	13.16	1136.80
M10	1.2	0.8	61.50	8.86	9.72	11.96	992.40

-Cost per 1 kg of steel fibers = 10000 I.D
-Cost per 1 kg of polypropylene fibers = 7000 I.D
-Cost per 1 kg of Epoxy = 18000 I.D

Step 1: Construct the decision matrix M: In this study, there are 10 alternatives (M1 to M10) and 5 criteria (Compressive Strength R1, Bond Strength R2, Flexural Strength R3, Toughness Indices R4, and Fiber Cost R5). Therefore, the common decision matrix can be expressed as:

$$M = \begin{bmatrix} m11 & m12 & m13 & m14 & m15 \\ m21 & m22 & m23 & m24 & m25 \\ \dots & \dots & \dots & \dots & \dots \\ \dots & \dots & \dots & \dots & \dots \\ \dots & \dots & \dots & \dots & \dots \\ m111 & m112 & m113 & m114 & m115 \end{bmatrix}. \quad (1)$$

In this study, decision-making problem can be expressed in matrix format as:

$$M = \begin{bmatrix} 65.2 & 9.38 & 15.04 & 9.22 & 785 \\ 67.2 & 9.27 & 15.59 & 10.10 & 942 \\ 69.7 & 9.70 & 15.62 & 10.90 & 1099 \\ 69.9 & 9.75 & 17.59 & 11.82 & 1256 \\ 71.6 & 10.08 & 17.63 & 13.10 & 1413 \\ 74.9 & 10.50 & 19.00 & 13.80 & 1570 \\ 70.0 & 10.17 & 17.20 & 16.61 & 1425.6 \\ 68.3 & 10.10 & 16.65 & 14.50 & 1281.2 \\ 64.3 & 9.56 & 14.30 & 13.16 & 1136.8 \\ 61.5 & 8.86 & 9.72 & 11.96 & 992.4 \end{bmatrix}. \quad (2)$$

Step 2: Establish the weighted normalized decision matrix N: The raw data need to be normalized using the following equation to eliminate anomalies with different measurement units and scales in several multi-criteria decision-making problems.

$$v_{ij} = \frac{m_{ij}}{\sqrt{\sum_{i=1}^{10} m_{ij}^2}}, \quad (i = 1, 2 \ldots 5, \quad j = 1, 2 \ldots\ldots 10) \tag{3}$$

Then the weighted normalized decision matrix can be computed by multiplying the importance weights of evaluation criteria and the normalized decision matrix.

$$n_{ij} = w_j \cdot v_{ij}, \tag{4}$$

where w_j is the importance weight of R_j and $\sum_{j=1}^{5} w_j = 1$.

In this study, the importance weights of evaluation criteria w_j for $R1$, $R2$, $R3$, $R4$, $R5$, are 0.2. Then the weighted normalized decision matrix N can be expressed as:

$$N = \begin{bmatrix} 0.0602 & 0.0609 & 0.0594 & 0.0460 & 0.0409 \\ 0.0621 & 0.0601 & 0.0615 & 0.0503 & 0.0491 \\ 0.0644 & 0.0629 & 0.0617 & 0.0543 & 0.0573 \\ 0.0646 & 0.0633 & 0.0694 & 0.0589 & 0.0655 \\ 0.0662 & 0.0654 & 0.0696 & 0.0653 & 0.0737 \\ 0.0692 & 0.0681 & 0.0750 & 0.0688 & 0.0819 \\ 0.0647 & 0.0660 & 0.0679 & 0.0828 & 0.0744 \\ 0.0631 & 0.0655 & 0.0657 & 0.0723 & 0.0668 \\ 0.0603 & 0.0620 & 0.0565 & 0.0656 & 0.0593 \\ 0.0568 & 0.0575 & 0.0384 & 0.0596 & 0.0518 \end{bmatrix}. \tag{5}$$

Step 3: Determine the positive and negative ideal reference points (A+ and A-): In this study, $R1$, $R2$, $R3$ and $R4$ are the benefit-type attributes I (the higher the better), while $R5$ is the cost-type attribute J (the lower the better). The positive ideal reference points A+ and negative ideal reference points A- can be expressed as:

$$A^+ = \{a1^+, a2^+, \ldots a5^+\} = \{(\max n_{ij} \mid j \in I), (\max n_{ij} \mid j \in J)\}, \tag{6}$$

$$A^+ = \{a1^-, a2^-, \ldots a5^-\} = \{(\max n_{ij} \mid j \in I), (\max n_{ij} \mid j \in J)\}. \tag{7}$$

Therefore, in this study, the positive ideal reference points A+ and negative ideal reference points A- can be calculated as:

$$A^+ = (0.0692, 0.0681, 0.0750, 0.0828, 0.0409), \tag{8}$$

$$A^- = (0.0568, 0.0575, 0.0384, 0.0460, 0.0819). \tag{9}$$

Step 4: Calculate the distance to positive and negative ideal reference point (d+ and d-): The distance of each value in the weighted normalized decision matrix to the positive ideal reference point and negative ideal reference point can be derived respectively as:

$$d + i = \sqrt{\sum_{j=1}^{5} (n_{ij} - a_j^+)^2}, \tag{10}$$

$$d - i = \sqrt{\sum_{j=1}^{5} (n_{ij} - a_j^-)^2}. \tag{11}$$

Therefore, in this study, the distance to positive ideal reference point d+ and the distance to negative ideal reference point d- can be calculated as:

$$d+ = \begin{bmatrix} 0.0416 \\ 0.0376 \\ 0.0361 \\ 0.0353 \\ 0.0378 \\ 0.0433 \\ 0.0345 \\ 0.0302 \\ 0.0330 \\ 0.0476 \end{bmatrix}, \quad d- = \begin{bmatrix} 0.0463 \\ 0.0408 \\ 0.0361 \\ 0.0387 \\ 0.0396 \\ 0.0461 \\ 0.0492 \\ 0.0421 \\ 0.0355 \\ 0.0331 \end{bmatrix}. \tag{12}$$

Step 5: Obtain the closeness coefficient r*: Once the distances to positive ideal reference point and the distance to negative ideal reference point are determined, the closeness coefficient r* can be obtained as:

$$r_i^* = \frac{(d_i^-)}{(d_i^+) + (d_i^-)}. \tag{13}$$

Therefore, in this study, the closeness coefficient r* can be calculated as:

$$r^* = \begin{bmatrix} 0.5263 \\ 0.5202 \\ 0.4999 \\ 0.5224 \\ 0.5117 \\ 0.5160 \\ 0.5876 \\ 0.5825 \\ 0.5176 \\ 0.4102 \end{bmatrix}. \tag{14}$$

A candidate fiber hybridization with an r* close to 1 has the shortest distance from the positive ideal reference point, and the largest distance from the negative ideal reference point. In other words, a large r* indicates good performance. The ascending rank of all the groups in this study is substituted as follows:

M7 > M8 > M1 > M4 > M2 >M9 > M6 > M5 > M3 > M10

The HPM reinforced by 1.8% steel fiber +0.2% polypropylene fiber "M7" having the largest closeness coefficient value, is the best among the ten mixes.

3.10. Bond strength results of the combined system

In this section, the evaluations of the selected mix in section 4.9 are presented. NC substrate are cast at 28-day earlier than the overlay mortar and the composite specimens were tested after curing period of 28-day. The results are presented in Figs. 19 and 20 with their details in Tables 11 and 12 for the two parts and three parts bond strength.

3.10.1. Effect of HPM on two-part bond strength

Table 11 contains the distinctive values for composite specimens involved: NC substrate bonded to reference

mix "R+M0", HPM reinforced by 2% mono steel fiber "R+M6" and HPM reinforced by 1.8% steel fiber + 0.2% polypropylene fiber "R+M7", with a sand blasting interfacial surface. The failure modes generally can be categorized into three types that is: 'Type A' is pure interfacial failure; 'Type B' is interfacial failure with partially substrate failure and 'Type C' is substratum failure as also supported by other study prepared by Tayeha et al. (2013).

The results present in Fig. 19 indicate a significant increase in slant shear strength and splitting tensile of HPM reinforced by 1.8% steel fiber + 0.2% polypropylene fiber "R + M7". This can be attributed to the efforts of steel fibers as well as polypropylene fibers to bridging the cracks and prevent the composite specimens from taking apart as reported by Chan and Chu (2004). On the other hand, the enhancement in bond strengths was less effective by using HPM reinforced by 2% steel fiber "R + M6" even though the fiber reinforcement prevents the composite specimens from separation. Consequently, the results show that the enhancement was less effective using reference mix "R + M0" and with the worse failure mode 'Type A' to use it as a repair material.

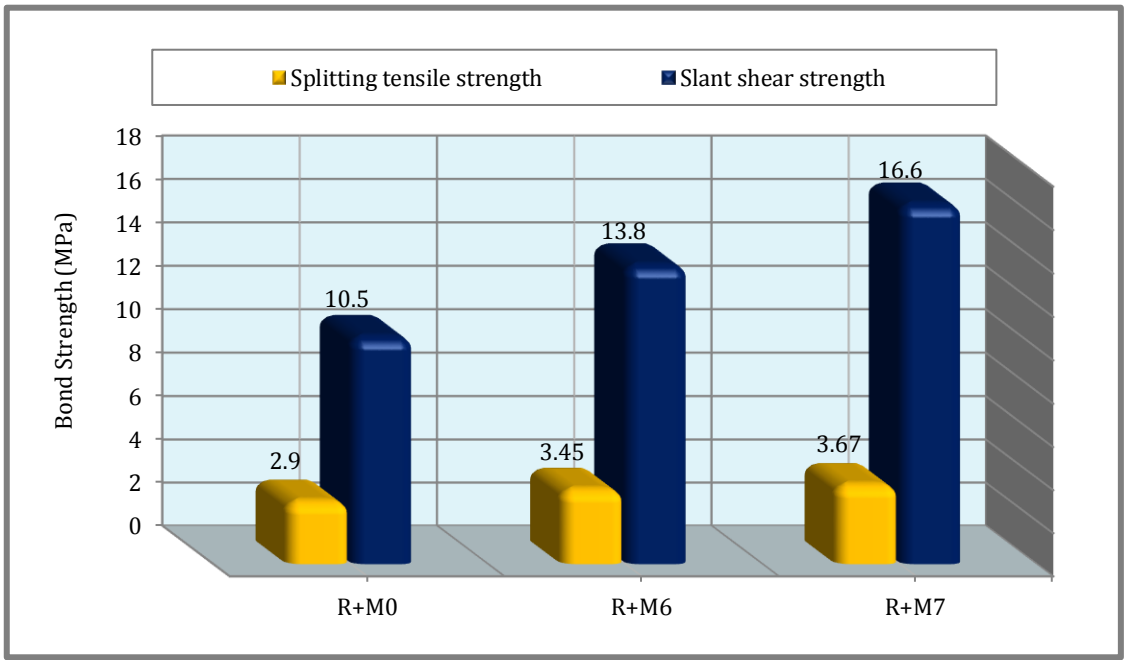

Fig. 19. Two parts bond strength.

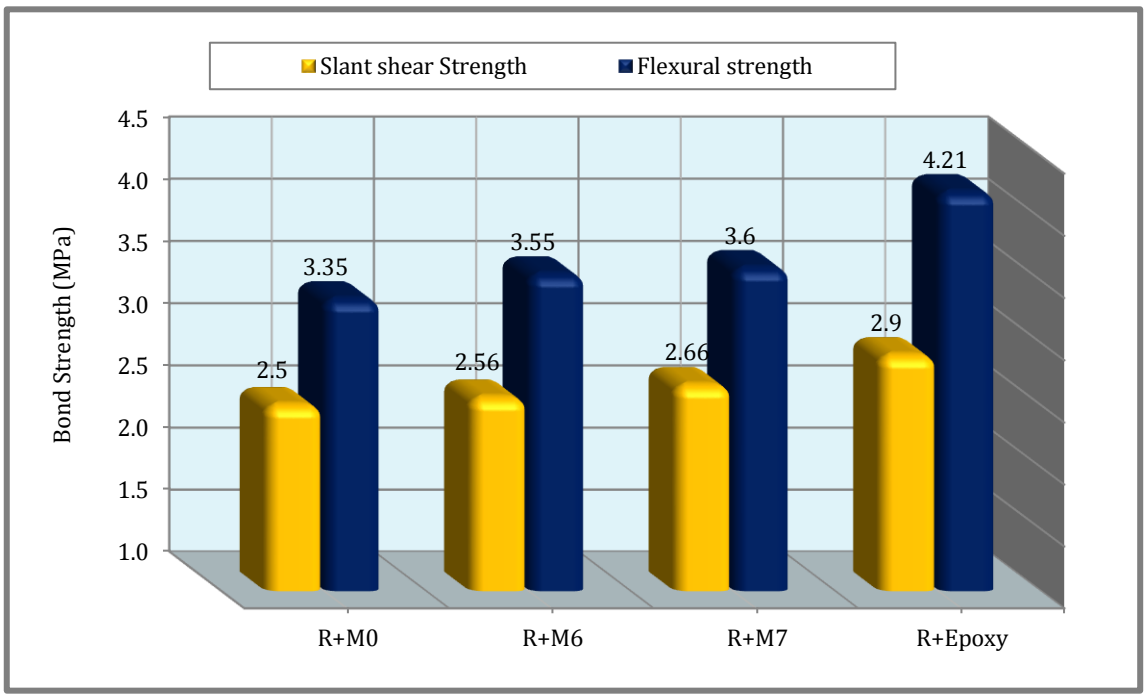

Fig. 20. Three parts bond strength.

Table 11. Properties of combined system [normal concrete + HPM mixes].

Index		Bond strength (Two-part)					
		Slant Shear Strength			Splitting Tensile Strength		
		Force (kN)	Strength (MPa)	Failure Mode*	Force (kN)	Strength (MPa)	Failure Mode*
R+M0	Sample 1	92.5	10.5	A	58.1	2.9	A
	Sample 2			B			A
R+M6	Sample 1	122.0	13.8	C	69.3	3.45	B
	Sample 2			C			B
R+M7	Sample 1	146.6	16.6	C	73.4	3.67	B
	Sample 2			C			B

*Failure mode:
Type A is pure interfacial failure; Type B is interfacial failure with partially substrate failure and Type C is substratum failure.

Table 12. Properties of combined system [normal concrete + HPM/epoxy].

Index		Bond strength (Three-part)					
		Slant Shear Strength			Flexural Strength		
		Force (kN)	Strength (MPa)	Failure Mode*	Force (kN)	Strength (MPa)	Failure Mode*
R+M0	Sample 1	44.9	2.5	A	12.1	3.35	A
	Sample 2			B			A
R+M6	Sample 1	45.4	2.56	C	12.7	3.5	B
	Sample 2			C			B
R+M7	Sample 1	47.1	2.66	C	13.1	3.60	B
	Sample 2			C			B
R+Epoxy	Sample 1	52.3	2.9	B	15.3	4.21	A
	Sample 2			B			A

*Failure mode:
Type A is pure interfacial failure; Type B is interfacial failure with partially substrate failure and Type C is substratum failure.

3.10.2. Effect of HPM on three-part bond strength

The results of slant shear strength and the flexural strength are very important in the evaluation of repair materials. Slant shear of full cylinder in addition to composite beam are measured after connecting two parts of NC substrate with the overlay layer of M0, M6 and M7 as well as the epoxy material. As the results illustrated in Table 12, the best value of slant shear strength is the value of 2.9 MPa from the combination of NC with epoxy and the interface failure occurred after the damage in the NC substrate 'Type B failure mode'. Slant shear strength was found 3.5 MPa and 3.6 MPa for "R+M6" and "R+M7" respectively and the failure occurred only in the NC substrate 'Type C' and there is no separation between the NC substrate and the HPM which indicates that superior bond behavior due to the presence of fibers. The least value was obtaining in the combination system with reference mix "R+M0" with 'Type A' failure mode.

For the flexural strength, Figure 20 shows the combination of NC substrate with epoxy boasts the best value of 4.21 MPa compare to other connect system although it shows 'Type A' failure mode. The performance of HPM reinforced with fiber was found to be lesser effective in improving than epoxy, although the presences of the fibers prevent the combined specimen from separation and be evidence for 'Type B' failure mode. The least value of composite beam strength was obtained by combinations with reference mix "R+M0".

In general, it can be concluded that HPM reinforced by hybrid fibers has the best performance when two-part bond strength is required. On the other hand, in three parts bonding, the connection of NC with epoxy has the best bond strength value while HPM reinforced fibers show a superior failure mode in view of the fact that there is no separation in the composite specimen.

4. Conclusions

Depending on the testing program of this investigation, the following conclusions can be drawn:

- Incorporation of metakaolin in HPM mixes at 10% as a partial replacement of cement gives the highest increase in compressive strength compared with other ratios of replacement.
- The inclusion of mono steel fibers has a lesser effect on the flowability of HPM compared with hybrid fibers (steel + polypropylene).
- The use of 2% steel fibers increases the compressive strength of HPM by about 14%. Whereas, the hybridization of 1.8% steel fibers + 0.2% polypropylene fibers gives the highest increment of 7% compared with the other hybridization mixes.
- The splitting tensile strengths of HPM are significantly improved by incorporating 2% of steel fiber. Thus, the splitting tensile strength of HPM has increased by about 18% higher than that of the control mix. However the inclusion of the hybrid fibers of 1.8% steel fiber plus 0.2% polypropylene fibers increase the splitting tensile strength by about 14%.
- The use of fibers increases the flexural strength of HPM. However, steel fibers show best performance compared with hybrid fibers. The highest increment of the flexural strength of HPM is 15% by the incorporation of 2.0% steel fibers.
- The toughness indices results show that the use of 2% of mono steel fiber boasts the highest performance compared with other mixes. On the other hand in the hybridization fiber, steel fibers provide reasonable first crack strength, while the polypropylene fibers improve toughness strength in the post-crack zone.
- Hybridization of 1.8% steel fiber + 0.2% polypropylene fiber performs the best result according to the TOPSIS method, which is very beneficial to decrease the production cost.
- The combined strength of two-part shows the use of HPM reinforced by 1.8% steel fibers + 0.2% polypropylene fibers exhibits better performance than that of other composite systems.
- Most of the failure mode in two-part bond tests was through the NC substrate specimen which indicated the bond strength between HPM and NC substrate is stronger than the cracking strength of the NC.
- The best value of three-part bond test was obtained by combination of NC substrate with epoxy as a repair material, while the least values was obtained from repair material using HPM.
- HPM reinforced with fibers show a superior failure mode in three-part bond test in view of the fact there is no separation in the composite specimens in contrast to epoxy combined system.

Acknowledgements

This work was prepared in the laboratory of Mosul Technical College. Big thanks are extended to the staff of Building and Construction Engineering Department, and to the staff of Technical Engineering Workshop for their support.

References

Abd ElAty MA (2013). Influence of bending deflection rate on properties of fibrous mortar. *HBRC Journal*, 9, 27–35.

ASTM C1018 (2002). Standard Test Method for Flexural Toughness and First-Crack Strength of Fiber-Reinforced Concrete (Using Beam with Third-Point Loading). Annual book of ASTM Standards.

ASTM C109 (2002). Standard Test Method for Compressive Strength of Hydraulic Cement Mortars (Using 2-in. or [50-mm] Cube Specimens). Annual book of ASTM Standards.

ASTM C230 (2002). Standard Specification for Flow Table for Use in Tests of Hydraulic Cement. Annual book of ASTM Standards.

ASTM C348 (2002). Standard Test Method for Flexural Strength of Hydraulic-Cement Mortars. Annual book of ASTM Standards.

ASTM C496 (2002). Standard Test Method for Splitting Tensile Strength of Cylindrical Concrete Specimens. Annual book of ASTM Standards.

ASTM C642 (2002). Standard Test Method for Density, Absorption, and Voids in Hardened Concrete. Annual book of ASTM Standards.

ASTM C78 (2002). Standard Test Method for Flexural Strength of Concrete (Using Simple Beam with Third-Point Loading). Annual book of ASTM Standards.

ASTM C882 (2002). Standard Test Method for Bond Strength of Epoxy-Resin Systems Used With Concrete by Slant Shear. Annual book of ASTM Standards.

Aydin A (2007). Self compactability of high volume hybrid fiber reinforced concrete. *Construction and Building Materials*, 21(6), 1149-1154.

Balaguru PN, Shah SP (1992). Fiber-Reinforced Cement Composites. McGraw-Hill Inc., New York.

Balendran R, Zhou F, Nadeem A, leung AYT (2002). Influence of steel fibres on strength and ductility of normal and lightweight high strength concrete. *Building and Environment*, 37, 1361-1367.

Banthia N, Sappakittipakorn M (2007). Toughness enhancement in steel fiber reinforced concrete through fiber hybridization. *Cement and Concrete Research*, 37(9), 1366-1372.

Bendjillalia K, Gouala MS, Chemrouk M, Damenea Z (2011). Study of the reinforcement of limestone mortars by polypropylene fibers waste. *Physics Procedia*, 21, 42–46.

Bentur A, Mindess S (1990). Fiber Reinforced Cementitious Composites. Elsevier Applied Science, London.

Campello E, Pereira MV, Darwisha F (2014). The effect of short metallic and polymeric fiber on the fracture behavior of cement mortar. *Procedia Materials Science*, 3, 1914–1921.

Chan YW, Chu SH (2004). Effect of silica fume on steel fiber bond characteristics in reactive powder concrete. *Cement and Concrete Research*, 34(7), 1167–1172.

Chynoweth G, Stankie RR, Allen WL, Anderson RR, Babcock WN, Barlow P (1996). Concrete Repair Guide. ACI Committee, Concrete Repair Manual, 546, 287-327.

Dawood ET, Ramli M (2010). Development of high strength flowable mortar with hybrid fibre. *Construction and Building Materials*, 24, 1043–1050.

Dawood ET, Ramli M (2011). High strength characteristics of cement mortar reinforced with hybrid fibres. *Construction and Building Materials*, 25, 2240–2247.

Dawood ET, Ramli M (2012). Mechanical properties of high strength flowing concrete with hybrid fibers. *Construction and Building Materials*, 28(1), 193-200.

Gwo-Hshiung, T, Jih-Jeng H (2011). Multiple Attribute Decision Making: Methods and Applications. Taylor and Francis Group, LLC, Boca Raton, FL, 69-76.

Haber ZB, Mackie KR, Zhao L (2012). Mechanical and environmental loading of concrete beams strengthened with epoxy and polyurethane matrix carbon fiber laminates. *Construction and Building Materials*, 26, 604–612.

Hsie M, Tu C, Song PS (2008). Mechanical properties of polypropylene hybrid fiber-reinforced concrete. *Materials Science and Engineering*, 494(1), 153-157.

Izaguirre A, Lanas J, Alvarez JI (2011). Effect of a polypropylene fibre on the behaviour of aerial lime-based mortars .*Construction and Building Materials*, 25, 992–1000.

Koksal F, Altum F, Yigit I, Sahin Y (2008). Combined effect of silica fume and steel fiber on the mechanical properties of high strength concretes. *Construction and Building Materials*, 22(8), 1874-1880.

Kuder K, Shah S (2010). Processing of high-performance fiber-reinforced cement based composites. *Construction and Building Materials*, 24, 181–186.

Lawler JS, Wilhelm T, Zampini D, Shah SP (2003). Fracture processes of hybrid fiber-reinforced mortar. *Materials and Structures / Matrriaux et Constructions*, 36, 197-208.

Liu CT, Huang JS (2008). Highly flowable reactive powder mortar as a repair material. *Construction and Building Materials,* 22(6), 1043–1050.

Mallat A, Alliche A (2011). Mechanical investigation of two fiber-reinforced repair mortars and the repaired system. *Construction and Building Materials*, 25, 1587–1595.

Markovic I, Walraven JC, Van MJ (2003). Self compacting hybrid fiber concrete-mix design, workability and mechanical properties. *Proceedings of Third International Symposium on Self-Compacting Concrete*, 763-775.

Mehta P, Monteiro P (2006). Concrete: Microstructure, Properties, and Materials. Third Edition. McGraw-Hill Inc., New York.

Miloud B (2005). Permeability and porosity characteristics of steel fiber reinforced concrete. *Asian Journal of Civil Engineering (Building and Housing)*, 6(4), 317-330.

Mohammadi Y, Singh SP, Kaushshik SK (2005). Properties of steel fibrous concrete containing mixed fibres in fresh and hardened state. *Construction and Building Materials*, 22(5), 956-965.

Momtazi AS, Zanoosh RZ (2011). The effects of polypropylene fibers and rubber particles on mechanical properties of cement composite containing rice husk ash. *Procedia Engineering*, 10, 3608–3615.

Mustafa S, Yaman OI (2007). Hybrid fiber reinforced self compacting concrete with a high volume coarse fly ash .*Construction and Building Materials*, 21, 150–156.

Natali A, Manzia S, Bignozzia MC (2011). Novel fiber-reinforced composite materials based on sustainable geopolymer matrix. *Procedia Engineering*, 21, 1124–1131.

Pattnaik RR (2006). Investigation into Compatibility between Repair Material and Substrate Concrete using Experimental and Finite Element Method. *Ph.D. thesis*, Graduate School of Clemson University.

Qureshi LA, Sheikh MI, Sultan T (2013). Effect of mixing fiber cocktail on flexural strength of concrete. *Procedia Engineering*, 54, 711–719.

Qureshia LA, Sheikh MI, Sultan T (2013). Effect of mixing fiber cocktail on flexural strength of concrete. *Procedia Engineering*, 54, 711–719.

Ramezanianpour AA, Jovein HB (2012). Influence of metakaolin as supplementary cementing material on strength and durability of concretes. *Construction and Building Materials*, 30, 470-479.

Sahmaran M, Yurtseven A, Yaman, OI (2005). Workability of hybrid fiber reinforced self-compacting concrete. *Building and Environment*, 40, 1672–1677.

Schueremans L, Cizer Ö, Janssens E, Serré G, Balen KV (2011). Characterization of repair mortars for the assessment of their compatibility in restoration projects: Research and practice. *Construction and Building Materials*, 25, 4338–4350.

Sevil T, Baran M, Bilir T, Canbay E (2011). Use of steel fiber reinforced mortar for seismic strengthening *Construction and Building Materials*, 25, 892–899.

Sivakumar A, Santhanam M (2007). Mechanical properties of high strength concrete reinforced with metallic and non-metallic fibres. *Cement and Concrete Composites*, 29, 603–608.

Steffen G, Joost CW (2001). Parameter study on the influence of steel fibers and coarse aggregate content on the fresh properties of self compacting concrete. *Cement and Concrete Research*, 3, 1793–1798.

Sun W, Chen H, Luo X, Qian H (2001). The effect of hybrid fibers and expansive agent on the shrinkage and permeability of high-performance concrete. *Cement and Concrete Research*, 31, 595–600.

Tayeha BA, Abu Bakarb BH, Megat Joharib MA, Vooc YL (2013). Evaluation of bond strength between normal concrete substrate and ultra high performance fiber concrete as a repair material. *Procedia Engineering*, 54, 554–563.

Tien-Chin W, Tsung-Han C (2007). Application of TOPSIS in evaluating initial training aircraft under a fuzzy environment. *Expert Systems with Applications*, 33, 870-880.

Yao W, Lib J, Wu K (2003). Mechanical properties of hybrid fibre reinforced concrete at low fibre volume fraction. *Cement and Concrete Research*, 33, 27–30.

.

Challenge Journal of Concrete Research Letters

Structural behaviour of ferrocement channels slabs for low cost housing

Yousry B. I. Shaheen [a,*], Essam A. Eltehawy [b]

[a] *Department of Civil Engineering, Menoufia University, Shebin ElKoum, Menofia, Egypt*
[b] *Department of Civil Engineering, Military Technical College, Cairo, Egypt*

ABSTRACT

This paper presents a new pre cast U-shape ferrocement forms reinforced with various types of metallic and non-metallic mesh reinforcement. This research was designed to investigate the feasibility and effectiveness of employing various types of reinforcing meshes in the construction of structural slabs incorporating permanent U-shape ferrocement forms as a viable alternative for conventional reinforced concrete slabs. Fiber glass meshes reinforcement was used for durability and protection against corrosion of reinforcing steel. To accomplish this objective, an experimental program was conducted. The experimental program comprised casting and testing ten slabs having the total dimensions of 500x100x2500 mm incorporating 40 mm thick U-shape permanent ferrocement forms. Series A consists of two conventionally reinforced concrete slabs were cast and tested and used as control slab without fibers and with fibers, volume fraction, 2.05 % and 2.177 %. Series B comprises of two slabs reinforced with one and two layers of expanded steel mesh, volume fraction 2.09 and 2.42% respectively. Series C comprises two slabs reinforced with two and four layers of welded galvanized steel mesh, having volume fraction 2.05 and 2.189% respectively. Series D Consists of two slabs reinforced with one layer and two layers of fiber glass meshes, having volume fraction 2.107 and 2.277% respectively. Series E comprises two slabs reinforced with 2 layers expanded steel mesh and one layer expanded steel mesh, having volume fraction 1.357 and 2.750 % respectively. The test specimens were tested as simple slabs under four-line loadings condition on a span of 2300mm. The performance of the test slabs in terms of strength, stiffness, strains, cracking behavior, ductility, and energy absorption properties was investigated. The behavior of the developed slabs was compared to that of the control slabs. The experimental results showed that high ultimate and serviceability loads, better crack resistance control, high ductility, and good energy absorption properties could be achieved by using the proposed slabs and low cost compared with control specimen.

ARTICLE INFO

Article history:
Received 7 March 2017
Accepted 15 May 2017

Keywords:
Ferrocement channels
Deformation characteristics
Serviceability load
Cracking behaviour
Ductility
Energy absorption

1. Introduction

Recently, ferrocement has emerged as new construction material. ACI defines ferrocement as follows: "Ferrocement is a type of reinforced concrete commonly constructed of hydraulic cement mortar reinforced with closely spaced layers of relatively small wire diameter mesh. The mesh may be made of metallic or other suitable materials. The fineness of the mortar matrix and its composition should be compatible with the opening and tightness of the reinforcing system it is meant to encapsulate. The matrix may contain discontinuous fibres (Naaman and Shah, 1971; ElMohimen, 2005).

1945 Nervi built the 165 ton Motor Yatch "Prune" on a supporting frame of 6.35 mm dia. rods spaced 106 mm apart with 4 layers of wire mesh on each side of rods with total thickness of 35 mm. It weighed 5% less than a comparable wooden hull & cost 40% less at that time.

* *Corresponding author*. Tel.: +020-128-2643204 ; E-mail address: ybishaheen@yahoo.com (Y. B. I. Shaheen)
ISSN: 2548-0928 / DOI: https://doi.org/10.20528/cjcrl.2017.02.002

The first ferrocement structure - a vaulted roof over shopping centre was built in Leningrad in Soviet Union In 1974, the American Concrete Institute formed committee 549 on ferrocement. In 1975, two ferrocement aqueducts were designed & built for rural irrigation in China (Channi, 2009).

Ferrocement is now recognized as a construction material with excellent qualities of crack control, impact resistance, and toughness, largely due to the close spacing and uniform dispersion of reinforcement within the material. Many investigations have clarified the physical and mechanical properties of this material, and numerous test data are available to define its performance criteria for design and construction (Rajagoplan and Parameswaran, 1975; Singh et al., 1986; Mansur and Paramasivam, 1990; Ramesht and Vickridge, 1996; Fahmy et al., 1997a, 1997b, 2004; Wrigley, 2001; El-Sakhawy, 2007).

Structural applications of ferrocement, boats, service evaluation of ferrocement boats, tanks, silos, roofs, ferrocement as a construction material, ferrocement for repair and strengthening of structures (Naaman and Shah, 1971; Sutherland, 1972; Swamy and Abboud, 1988; Fahmy and Shaheen, 1991; Fahmy et. al., 1995, 1997a, 1997b, 1999; El-Halfawy, 2003; Ayoub, 2005; Tomar, 2006).

The successful usage of ferrocement in repairing and construction of reinforced concrete beams and the high cost of traditional wooden or steel form work led to the idea of using ferrocement laminate as permanent forms in concrete construction (Rosenthal and Bljuger, 1985; Rao and Rao, 1987; Swamy and Abboud, 1988; Abdul Kadir and Jafaar, 1993; Mays and Barnes, 1995; Abdul Kadir et. al. 1997; ACI 549-1R-88, 1998; Wrigley, 2001; Housing and Building Research Center, 2001; El-Halfawy, 2003; Abdel Tawab, 2006).

Abdul Kadir and Jaafar (1993) offered a proposed technique for using ferrocement concept to produce in situ permanent formwork as a viable alternative of traditionally used wooden forms. Ferrocement permanent formwork has great potentials in reducing construction time especially for curved structures, saving timber, and minimizing cost. It also reduces the tensile steel as a result of utilizing steel mesh which contributes also the flexural strength of the beams.

Mays and Barnes (1995) presented the results of an experimental investigation the feasibility of using pre cast ferrocement as a low permeability cover layer to the subsequently poured in situ reinforced concrete members located in environments, where there is a high risk of reinforcement corrosion. The research focused particularly on achieving an adequate and durable bond between the ferrocement layer and the concrete core in order to develop composite structural behaviour. They concluded that not only the resistance to chloride penetration was enhanced by using Styrene Butadiene Rubber (SBR) or acrylic bond coat between the ferrocement forms and the concrete, but also the use of permanent ferrocement formwork provided an increase in strength of 15% over the conventional reinforced concrete.

Abdul Kadir et al. (1997) presented the results of test on the flexural behaviour of reinforced concrete beams with ferrocement permanent formwork. One contained eight beams without mechanical shear connection between the ferrocement forms and the concrete core. And the other contained eight beams in which shear connectors shaped as 12mm × 22mm rectangular humps were placed at every 22mm centres. The area of the steel mesh was maintained constant at 55mm^2 for all beams while the area of reinforcing bars in the concrete core was variable. The results showed that the reinforced concrete beams with ferrocement permanent formwork failed by flexure under two point load test. The beams incorporating ferrocement formwork contributed from 16 to 75% to the flexural strength of the composite beams depending on steel area and the use of shear connectors. The ferrocement forms incorporating reinforced concrete core with shear connectors achieved higher strength by an average of 10% compared to the ones without shear connectors; however, they showed lower deflections when subjected to the same load.

Housing demand is rising because of the increasing population, but the high construction cost is important factor in the development of building industry. In order to balance the demand and cost for viable development of building industry, new building materials and methodology has to be developed. Ferrocement has the potential to solve many problems, technical and economic. In the construction of different types of housing systems. Housing shortages have become a dramatic fact of life in the world today. As housing demand and cost of construction both increase. Ferrocement is an excellent material for use in housing construction mainly for roofing because of its relatively low cost, durability and weather resistance. Particularly the versatility of the material further increase its utility for producing components required in housing. A ferrocement shell roof is a good example of its use in housing because of its water tightness. Unlike most conventional materials, ferrocement can be easily shaped into domes, vaults, and extruded type shapes, flat surfaces. It can span long distance and thus reduce the need for closely supports. Prefabricated ferrocement roofing elements can be produced in very interesting architectural shapes either at a factory or in site to provide relatively light roofing structures for low cost houses. The use of precast ferrocement dome and shell roofing components should be encouraged. However, attention must be given to proper detailing of joints between the roofing elements to avoid problem of water leakage through the joints.

Abdel Tawab (2006) presented the results of an investigation aiming at the development of U-shaped ferrocement permanent forms to be used for construction of reinforced concrete beams as a viable alternative to traditionally used wooden and metal formwork. The test parameters were the type of steel mesh, number of steel mesh layers. The performance of the test beams in terms of: strength, stiffness, cracking behaviour, ductility, and energy absorption properties was investigated. The results showed that high ultimate and serviceability loads, crack resistance control, high ductility, and good energy absorption properties could be achieved by using the proposed permanent ferrocement forms.

2. Experimental Program

The experimental program was divided into two phases, the first phase regarding the reinforcement; the main objective was to determine the mechanical properties of the used steel and wire meshes. The second phase, the main objective was studying the ultimate load, flexural behaviour, ductility ratio, energy absorption and mode of failure at collapse of the control slabs, which were reinforced with steel bars and u shape steel stirrups and to compare their behaviour with those reinforced ferrocement slabs reinforced with expanded metal mesh and welded galvanized steel mesh and glass fibre mesh. Skeletal steel bars and steel stirrups were used with steel meshes and fiber glass mesh. Table 1 presents details of experimental program.

In this program, ten specimens were cast and tested in order to study their behaviour under flexural loadings. Table 1 shows details of the experimental program of all the test specimens while Fig. 1 emphasizes the types of meshes and polypropylene fibers used. Fig. 2 shows reinforcement configurations details of all U shape control slabs and ferrocement channels. Fig. 3 shows photos of reinforcement configurations of all U shape slabs.

Table 1. Details of experimental program.

Series Designation	Slab No.	Volume fraction of reinforcement, %	Reinforcement details			
			Tension Steel bars, Ø 10 mm	Compression Steel bars, Ø 6 mm	No. of Stirrups, Ø 6 mm	No. and Type of Mesh Layers
A	1	2.05	4	2	15	------
	2	2.177	4	2	15	------
B	3	2.09	4	2	2	1 Layer Expanded Steel Mesh
	4	2.42	4	2	--	2 Layers Expanded Steel Mesh
C	5	2.05	4	2	4	2 Layers Welded Steel Mesh
	6	2.189	4	2	2	4 Layers Welded Steel Mesh
D	7	2.017	4	2	4	1 Layer Fibre Glass Mesh
	8	2.277	4	2	4	2 Layers Fibre Glass Mesh
E	9	1.357	--	2	--	2 Layers Expanded Steel Mesh
	10	2.750	6	2	--	1 Layer Expanded Steel Mesh

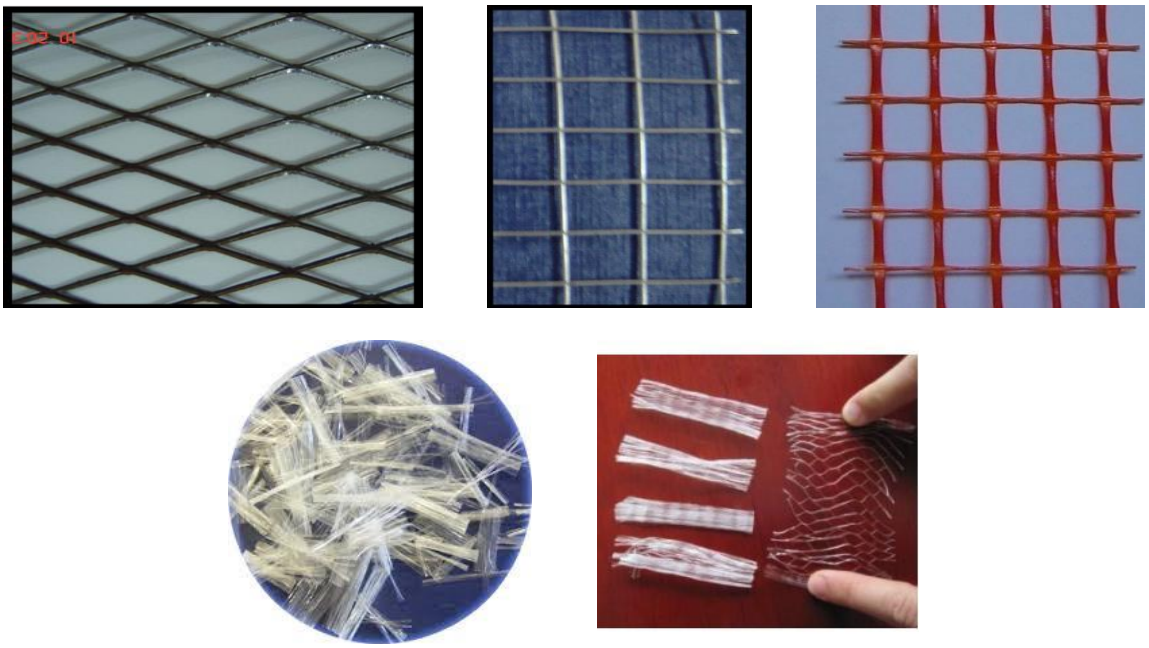

Fig. 1. Types of meshes and fibres used.

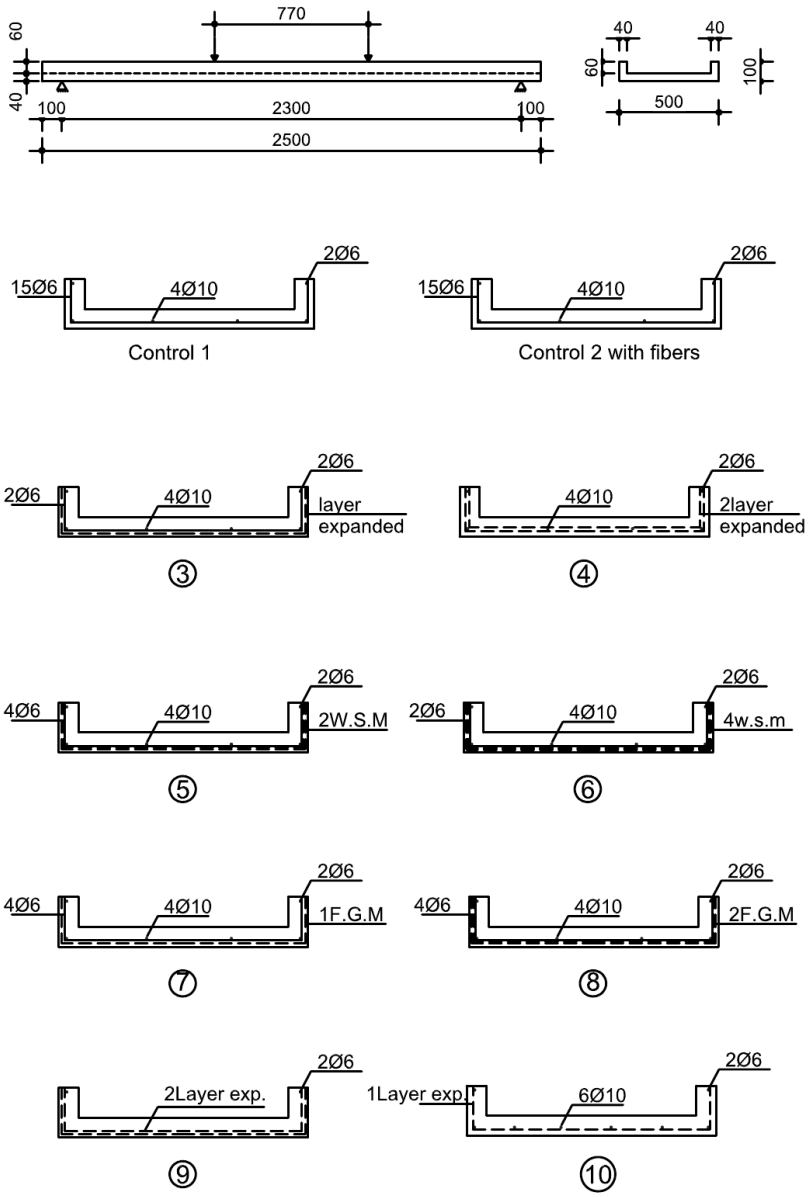

Fig. 2. Reinforcement details of all slabs.

2.1. Materials

- **The fine aggregate** used in the experimental program was of natural siliceous sand. Its characteristics satisfy the E.C.P. 203/2007 (Swamy et al, 1988) and E.S.S. 1109/2008 (Sandowicz et al., 1985). It was clean and nearly free from impurities with a specific gravity 2.6 t/m^3 and a modulus of fineness 2.7.
- **The cement** used was the Ordinary Portland cement, type produced by the Suez cement factory. Its chemical and physical characteristics satisfied the Egyptian Standard Specification E.S.S. 4657-1/2009 (Ayoub, 2005).
- **The water** used was the clean drinking fresh water free from impurities used for mixing and curing the R.C. beams tested according to the E.C.P. 203/2007 (Swamy et al., 1988).
- **Super plasticizer** used was a high rang water reducer HRWR. It was used to improve the workability of the mix. The admixture used was produced by CMB GROUP under the commercial name of Addicrete BVF. It meets the requirements of ASTM C494 (type A and F) (Singh et al., 1986). The admixture is a brown liquid having a density of 1.18 kg/litre at room temperature. The amount of HRWR was 1.0% of the cement weight.
- **Reinforcing steel**; Normal mild steel bars were used, produced from the Ezz Al Dekhila Steel - Alexandria Its chemical and physical characteristics satisfy the Egyptian Standard Specification E.S.S. 262/2011 (Sutherland, 1972). Mild steel bars of 6 mm diameter were used for stirrups with yield strength of 240 MPa.
- **Reinforcing meshes**

– **Expanded metal mesh**: Expanded metal mesh was used as reinforcement for ferrocement channels. The technical specifications and mechanical properties of expanded metal mesh as provided by producing company are given in Table 2. Fig. 1 illustrates the photo of the expanded metal mesh.

– **Welded metal mesh**: Galvanized welded metal mesh used was obtained from China. Welded metal mesh was used as reinforcement for ferrocement channels. The

technical specifications and mechanical properties of welded metal mesh as provided by producing company are given in Table 2. Fig. 1 illustrates the image.

– **Fibreglass mesh**: Fibreglass mesh used was obtained from Gavazzi Company, Italy, It was available in the Egyptian markets, The technical specifications and mechanical properties of Fibreglass mesh as provided by producing company are given in Table 2. Fig. 1 illustrates the image.

• **Polypropylene fibres** PP 300-e3 was used. It was available in the Egyptian markets. It was used in concrete mixes to produce fibrous concrete jacket to improve the concrete characteristics. The percentage of addition was chosen as 900 gm/m^3 based on the recommendations of manufacture. The technical specifications and mechanical properties of Polypropylene fibres PP 300-e3 as provided by producing company are given in Table 3. Fig. 1 illustrates the image.

Fig. 3. Reinforcement configuration of U shape slabs.

2.2. Mortar matrix

The concrete mortar used for casting channels was designed to get an ultimate compressive strength at 28-days age of (350 kg/cm^2), 35 MPa. The mix properties for mortar matrix were chosen based on the ACI Committee 549 Report (1988). For all mixes, mechanical mixer in the laboratory used mechanical mixing with capacity of 0.05 m^3, where the volume of the mixed materials was found to be within this range.

The constituent materials were first dry mixed; the mix water was added and the whole patch was re-mixed again in the mixer. The mechanical compaction was applied for all specimens. Mix proportions by weight for the different groups are given below in Table 4. Fig. 1 emphasizes the types of meshes used. Fig. 2 shows reinforcement details and photos of all control and ferrocement channels.

Table 2. Technical specifications and mechanical properties of expanded metal mesh and welded metal mesh.

Expanded Metal Mesh		Welded Metal Mesh		Fibreglass Mesh		
Style	1532	Dimensions Size	12.5×12.5 mm	Dimensions Size	12.5×11.5 mm	
Sheet Size	1×10 m	Weight	430 g/m^2	Dimensions of Strings	Longitudinal	1.66×0.66 mm
Weight	1.3 kg/m^2	Proof Stress	400 N/mm^2		Transverse	1×0.5 mm
Diamond Size	16×31 mm	Ultimate Strength	600 N/mm^2	Weight	123 g/m^2	
Dimensions of Strand	1.25×1.5 mm	Ultimate Strain	58.8×10^{-3}	Volume Fraction	0.535%	
Proof Stress	199 N/mm^2	Proof Strain	1.17×10^{-3}	Tensile Strength	325 N/mm^2	
Proof Strain	9.7×10^{-3}			Elongation	5.5%	
Ultimate Strength	320 N/mm^2					
Ultimate Strain	59.2×10^{-3}					

Table 3. Physical and mechanical properties of polypropylene fibers 300-e3.

Fiber Length	Type / Shape	Absorption	Specific Gravity	Electrical Conductivity	Acid &Salt Resistance	Melt Point	Ignition Point	Thermal Conductivity	Alkali Resistance
Various	Graded / Fibrillated	Nil	0.91	Low	High	162°C (324°F)	593°C (1100°F)	Low	Alkali Proof

Table 4. Ferrocement mortar mix proportions by weight/m^3.

Mix. Designation	Cement (kg)	SF. (kg)	PFA (kg)	Sand (kg)	Water (kg)	Super plasticizer	Fibres (kg)
M	408	68	204	1360	238	6.8	0.9

2.3. Volume fraction of reinforcement (V_r%)

Volume fraction of reinforcement is the total volume of reinforcement per unit volume of ferrocement. For a composite reinforced with meshes with square openings, (V_r) is equally divided into (V_{rt}) and (V_{ri}) for the longitudinal and transverse directions, respectively (Rao and Rao, 1987; Rosenthal and Bljuger, 1985).

2.4. Preparation of test specimens

A special wooden mold, Fig. 4, was designed and manufactured to cast U-shaped ferrocement forms .The ferrocement U-shaped forms were prepared in the following sequence:

1. The wooden mold was assembled and the reinforcing steel mesh was formed in a U-shaped form and the steel bars of 6 mm diameter were tight with steel mesh inside the ferrocement U-shaped forms and placed in the vent of the mold. The constituents of the mortar were mixed and cast in each vent to the required thickness of 25 mm.

2. Wooden pans were placed on top of the cast ferrocement layer and the sides of the ferrocement forms were cast around the wooden pans in the vent of the wooden mold.

3. The ferrocement forms were left for 24 hours in the mold before disassembling the mold. At the end of this step, three U-shaped ferrocement forms are produced. The forms were covered with wet burlap for 28 days.

2.5. Test setup

At the time of testing, the specimen was painted with white paint to facilitate the visual crack detection during testing process. A set of eight "demec" points was placed on one side of the specimen to allow measuring the strain versus load during the test. Demec points were placed as shown in Fig. 5.

The specimen was laid on a universal testing machine of maximum capacity of 100 kN, where the test was conducted under a four-point loads system with a span of 1800 mm. Three dial gauges with an accuracy of 0.01 mm were placed under the test specimen at the center to measure the deflection versus load. Load was applied at 5 kN increments on the specimen exactly at the center. The horizontal distance between each pair of demec points was recorded by using a mechanical strain gauge reader. Concurrently, the beam deflections were determined by recording the dial gauge reading at each load increment. Cracks were traced throughout the sides of the specimen and then marked with red and black markers. The first crack-load of each specimen was recorded. The load was increased until complete failure of the specimen was reached. Fig. 6 shows the test setup.

Fig. 4. U shape wooden mold.

Fig. 5. Demec sets.

Fig. 6. Test setup.

3. Experimental Results and Discussions

The experimental results of the test program and the discussions are presented. Comparisons are conducted between the results of the different test groups to examine the effect of the test parameters under investigation; existence of the permanent ferrocement forms, type of mesh reinforcement. The effects of these parameters on the structural responses of the proposed beams in terms of failure load, mode of failure, first crack load, service load, ductility ratio, and energy absorption were studied extensively. Table 5 presents First crack, serviceability, ultimate loads, ductility ratio and energy absorption properties of all the tested slabs.

Table 5. First crack, serviceability, ultimate loads, ductility ratio and energy absorption properties of all the tested slabs.

Slab No	First crack load (kN)	Service load (kN)	Ultimate Load (kN)	Def. at F.C.L (mm)	Def. at Ult. Load (mm)	Ductility ratio	Energy Absorption (kN·mm)
S1 control	10	10.56	19	16.45	32.15	1.95	393.98
S2 control	15	13.25	23.3	22	41.94	1.91	600.54
S3	15	10.68	19.17	19.11	30.58	1.60	413.8
S4	15	12.43	22	15.2	35.5	2.34	463.3
S5	15	14.19	24.8	17.1	32.2	1.88	509.28
S6	18	16.19	28	18.5	25.9	1.4	587.15
S7	15	9.38	17.1	28.32	34.7	1.23	372.72
S8	15	11.81	21	25.3	38.3	1.51	495.65
S9	15	8.75	16.1	27.36	36.89	1.35	395.87
S10	18	14.31	25	35.1	43.2	1.23	529.6

3.1. Flexural serviceability load

The flexural serviceability load was calculated from the load-deflection curves. It is defined as the load corresponding to deflection equal to the span of the slab (2300 mm) divided by (constant=250) according to The Egyptian Code. Fig. 7 represents the values for the first cracking load, serviceability load and ultimate load for all the tested slabs. Maximum ultimate load reached 28 kN for S6 and minimum ultimate load achieved 19 kN for control slab S1.

3.2. Ductility ratio

The ductility ratio was calculated as the mid span deflection at the ultimate load to that of the first cracking load. Slabs reinforced with expanded metal mesh and welded steel mesh were given higher ductility ratio than control beam. Slabs S9 and S10 were given lower ductility ratio than control slabs. Fig. 8 shows ductility ratios for all tested slabs.

3.3. Energy absorption

The energy absorption was obtained by calculating the area under the load-deflection curve for each slab. Slabs reinforced with expanded steel mesh were achieved higher energy absorption than control slab. Slabs reinforced with welded metal mesh reached higher energy absorption than control slab. Fig. 9 emphasises energy absorption for all tested slabs. Higher ductility and energy absorption properties are very useful for dynamic applications.

3.4. Behaviour of the test specimens

The behaviour of the test specimens in terms of load-deflection relationship, cracking behaviour, and mode of failure is discussed in the following sections.

3.4.1. Load-Deflection relationship

The load-deflection curves of the control specimen (S1 and S2), the specimens incorporating ferrocement forms and reinforced with expanded steel mesh (designations S3 and S4, reinforced welded wire mesh (designations S5 and S6) and those reinforced with Fiberglass mesh (designations S7 and S8). Ferrocement channels (S9 and S10) reinforced expanded steel mesh and steel bars. Figs. 10-14 show load deflection curves for all the test specimens while Fig. 15 emphasises comparison of load deflection curves for all the tested channels.

The load-deflection relationship for the control specimens was linear up to a load of 10-15 kN approximately after which the relation became non-linear. For this group of specimens, the transition from the second to the third stages, as explained before, was not distinct as shown in Fig. 10. At failure, the mid-span deflection reached 37.9 mm, and 44.5 mm for specimens S1 and, S2 respectively. And the ultimate load was 19 and 23.3 for S1 and, S2, respectively. S2 is higher than S1 as a result of the effect of polypropylene fibres employed.

For group B (designations S3 and S4) specimens reinforced with single layer of expanded wire mesh and two layers of expanded steel mesh respectively., The load-deflection relationship was almost linear up to load of about 15 kN and 15 kN for specimens S3 and S4 respectively when the deviation from the linear relation started. Maximum deflection reached 35.5 mm and 36 mm for specimens S3 and S4 respectively (Fig. 11). For group C, when S5 and S6 specimens reinforced with double layers of welded wire mesh and four layers of welded steel mesh respectively. The load-deflection relationship was almost linear up to load of about 15 kN and 18 kN respectively for specimens S5 and S6 respectively when the deviation from the linear relation started as shown in Fig. 12. At failure, the deflection reached 37 mm, 38.7 mm for slabs S5 and S6, respectively.

For group D (designations S7 and S8) specimens reinforced with one layer of fibre glass mesh and two layers of fibre glass mesh respectively, the load-deflection relationship was almost linear up to load of about 15 kN and 15 kN when the deviation from the linear relation started as shown in Fig. 13. At failure, the deflection reached 40.5 mm and 42.6 mm for slabs S7 and S8, respectively. For group E (S9 and S10) specimen reinforced with double layers of expanded steel mesh and one layer expanded steel mesh with skeletal steel bars, the load-deflection relationship was almost linear up to load of about 15 kN and 18 kN respectively when the deviation from the linear relation started as shown in Fig. 14. At failure, the deflection reached 40.9 mm and 47.6 mm, respectively.

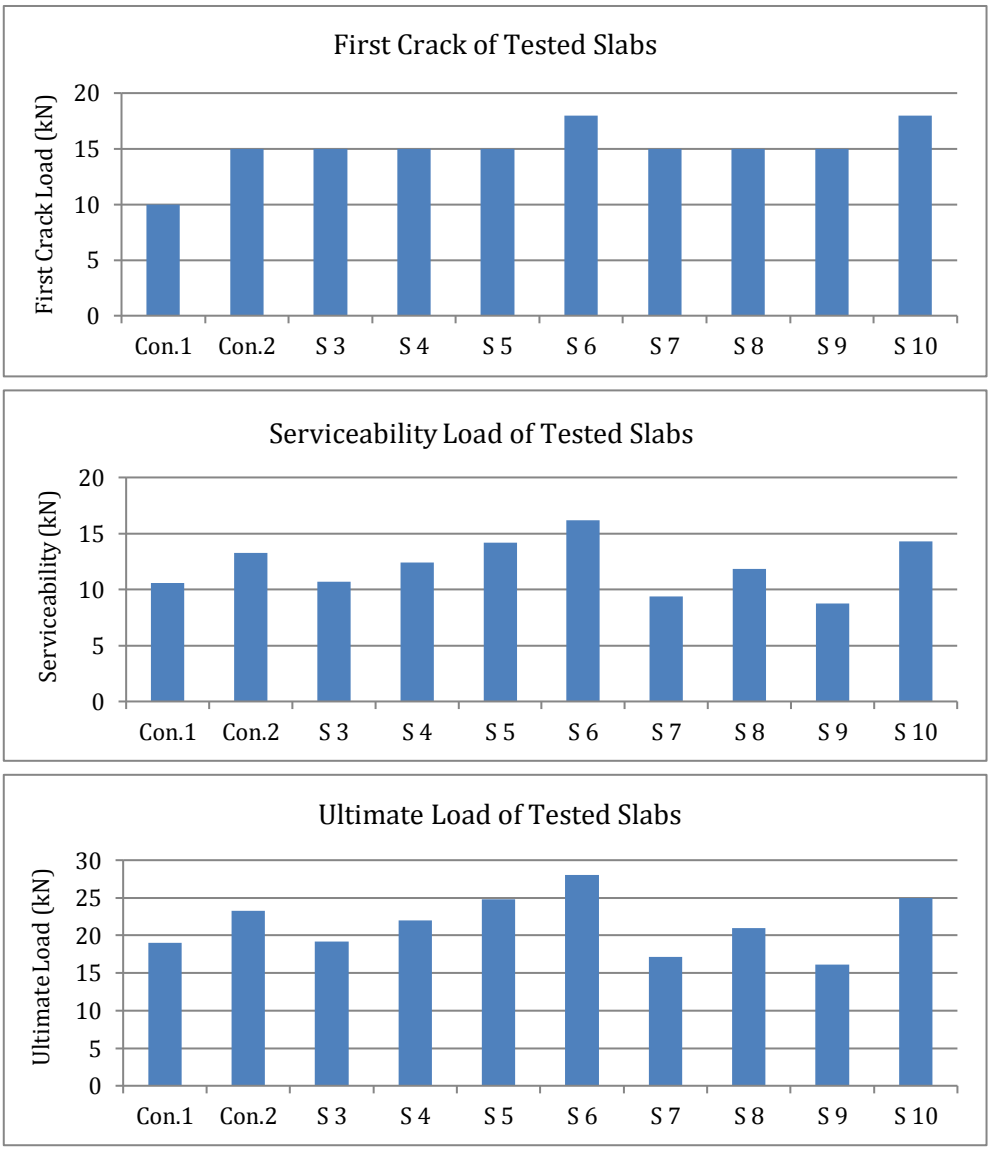

Fig. 7. First crack, serviceability and ultimate loads of all tested slabs.

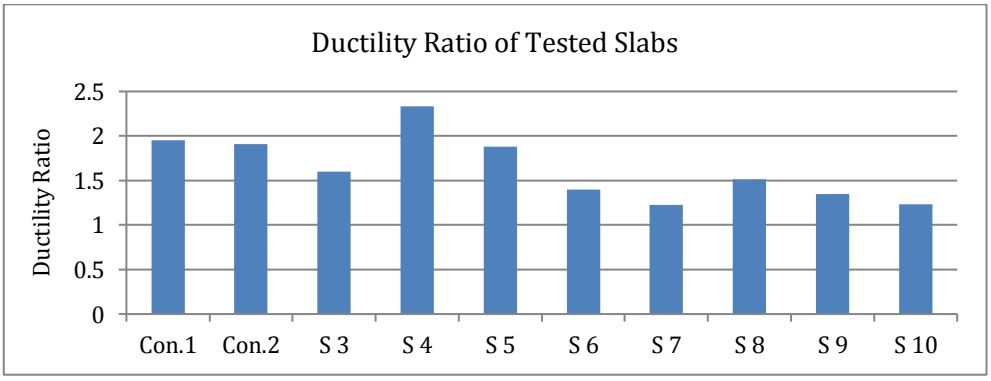

Fig. 8. Ductility ratios for all tested slabs.

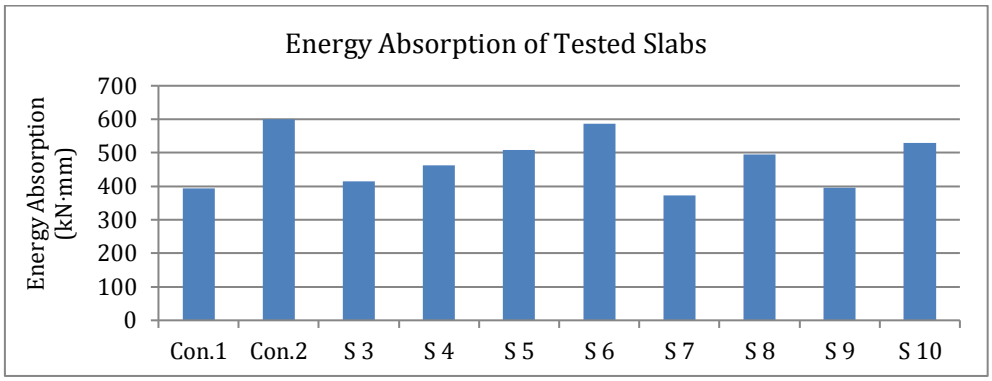

Fig. 9. Energy absorption for all tested slabs.

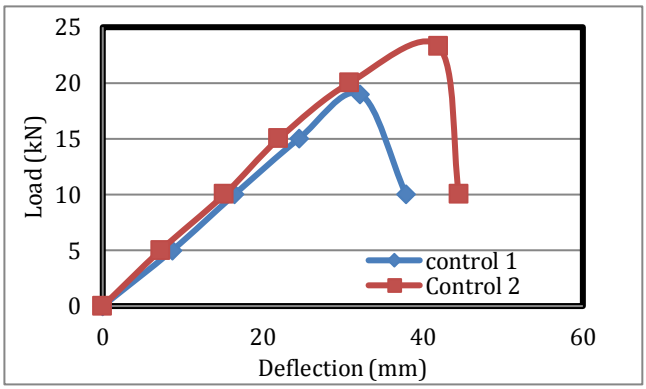

Fig. 10. Load-Deflection curves for group A.

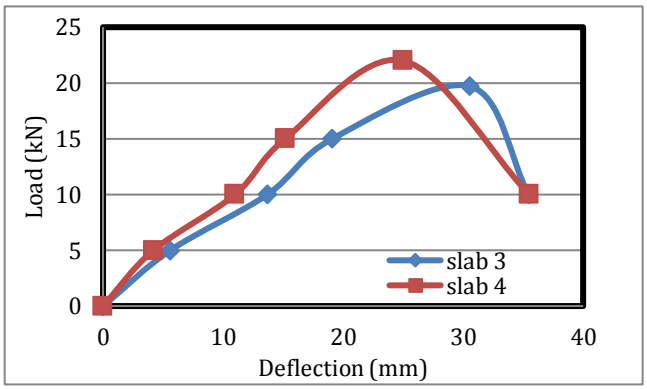

Fig. 11. Load-Deflection curves for group B.

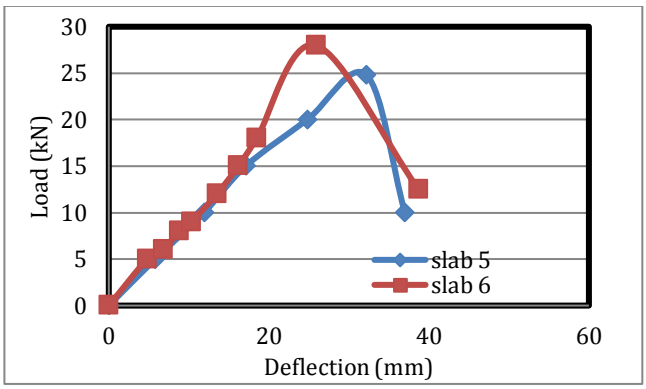

Fig. 12. Load-Deflection curves for group C.

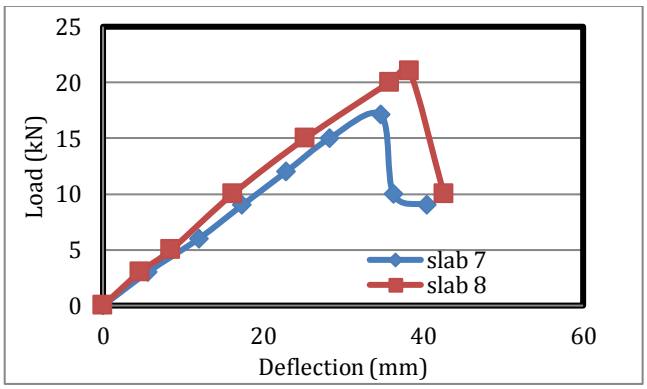

Fig. 13. Load-Deflection curves for group D.

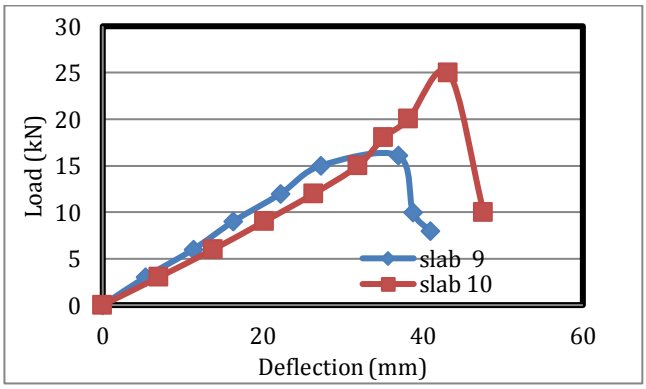

Fig. 14. Load-Deflection curves for group E.

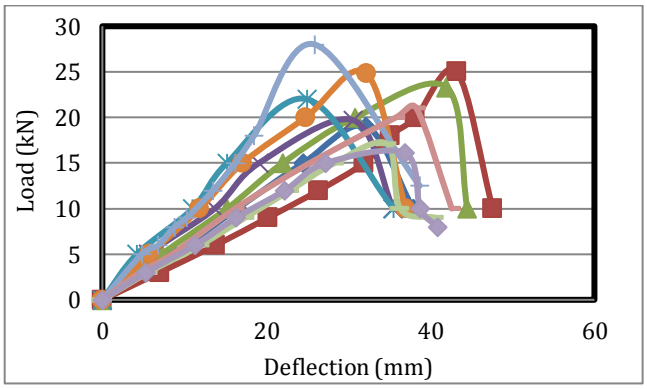

Fig. 15. Load-Deflection curves for all slabs.

3.4.2. Concrete strain

For Control A group specimens, S1 and S2. For slab S1, the compressive strain at the gauge location increased with the increase of the applied load. The maximum compressive strain at this location reached about -0.0038 strain at maximum load 19 kN. The compressive strain at gauge location number 2 followed similar trend. However, the strain at this location was less than that at location number 1 as shown from Fig. 16.

For slab S2, the compressive strain at the gauge location increased with the increase of the applied load. The maximum compressive strain at this location reached about -0.0048 strain at maximum load 23.3 kN. The compressive strain at gauge location number 2 followed similar trend. However, the strain at this location was less than that at location number 1 as shown from Fig. 17. The tensile strains at locations number 3 and 4 increased with the increase of the applied load with the strain at location number 3 being less than that at location number 4. At failure, the tensile strain reading reached 0.00429 strain at location number 4 as shown from Fig. 17.

For group B (S3, S4) specimens reinforced with single layer of expanded wire mesh, the compressive strain at the gauge location (location no. 1) increased almost linearly up to load of 15 kN when deviation from the linear relationship started as shown in Fig. 18. The maximum compressive strain at this location reached about -0.0038 strain at a load of 19.7 kN. The compressive strain at gauge location number 2 followed similar trend. However, the strain at this location was less than that at location number 1. The tensile strains at locations number 3 and 4 increased with the increase of the applied load with the strain at location number 3 being less than that at location number 4. At failure, the tensile strain reading reached 0.004015 strains at location number 4.

For S4, specimens reinforced with double layer of expanded wire mesh, the compressive strain at the gauge location (location no.1) increased almost linearly up to load of 15 kN when deviation from the linear relationship started as shown in Fig. 19. The maximum compressive strain at this location reached about -0.003 strain at a load of 22 kN. The compressive strain at gauge location number 2 followed similar trend. However, the strain at this location was less than that at location number 1. The tensile strains at locations number 3 and 4 increased with the increase of the applied load with the strain at location number 3 being less than that at location number 4. At failure, the tensile strain reading reached 0.001339 strains at location number 4.

For group C (designations S5 and S6) specimens S5 reinforced with two layer of welded wire mesh, the maximum compressive strain at this location reached about -0.002 strain at a load of 24.8 kN. The compressive strain at gauge location number 2 followed similar trend. However, the strain at this location was less than that at location number 1 as shown in Fig. 20. The tensile strains at locations number 3 and 4 increased with the increase of the applied load with the strain at location number 3 being less than that at location number 4. At failure, the tensile strain reading reached 0.002343 strain at location number 4 as shown in Fig. 20.

For specimen S6, reinforced with four layers of welded wire mesh, the compressive strain at the gauge location (location no. 1) increased with the increase of the applied load. The maximum compressive strain at this location reached about -0.0037 strain at load 28 kN. The tensile strains at locations number 3 and 4 increased with the increase of the applied load with the strain at location number 3 being less than that at location number 4. At failure, the tensile strain reading reached 0.0099 strain at location number 4. Fig. 21 shows load strain curves for slab S6.

For group D (designations S7 and S8). Specimens S7 reinforced with single layer of fiberglass mesh, the maximum compressive strain at this location reached about -0.0031 strain at a load of 17.1 kN. The compressive strain at gauge location number 2 followed similar trend. However, the strain at this location was less than that at location number 1. The tensile strains at locations number 3 and 4 increased with the increase of the applied load with the strain at location number 3 being less than that at location number 4. At failure, the tensile strain reading reached 0.004304 strain at location number 4. Fig. 22 shows load strain curves for slab S7.

Specimens S8 reinforced with double layers of fiberglass mesh, the maximum compressive strain at this location reached about -0.0034 strain at a load of 21 kN. The compressive strain at gauge location number 2 followed similar trend. However, the strain at this location was less than that at location number 1. The tensile strains at locations number 3 and 4 increased with the increase of the applied load with the strain at location number 3 being less than that at location number 4. At failure, the tensile strain reading reached 0.00418 strain at location number 4. Fig. 23 shows load strain curves for slab S8.

For group E (designations S9 and S10) Slab S9 reinforced with double layers of expanded steel mesh, the maximum compressive strain at this location reached about -0.00207 strain at a load of 16.1 kN. The compressive strain at gauge location number 2 followed similar trend. However, the strain at this location was less than that at location number 1. The tensile strains at locations number 3 and 4 increased with the increase of the applied load with the strain at location number 3 being less than that at location number 4. At failure, the tensile strain reading reached 0.001532 strains at location number 4. Fig. 24 shows load strain curves for slab S9.

Slab S10 reinforced with one layer of expanded steel mesh and skeletal steel bars. The maximum compressive strain at this location reached about -0.0043 strain at a load of 25 kN. The compressive strain at gauge location number 2 followed similar trend. However, the strain at this location was less than that at location number 1. The tensile strains at locations number 3 and 4 increased with the increase of the applied load with the strain at location number 3 being less than that at location number 4. At failure, the tensile strain reading reached 0.00397 strains at location number 4. Fig. 25 shows load strain curves for slab S9.

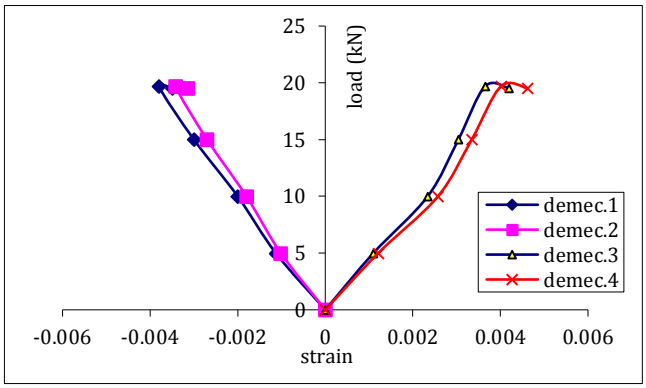

Fig. 16. Load-Strain curve of S1.

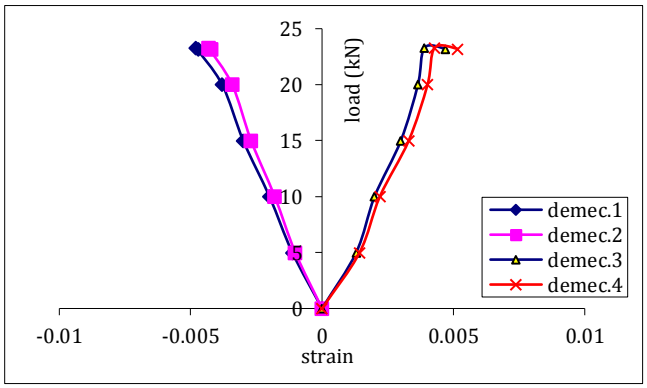

Fig. 17. Load-Strain curve of S2.

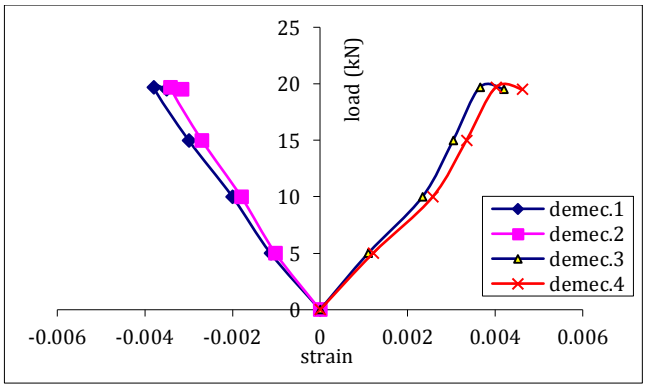

Fig. 18. Load-Strain curve of S3.

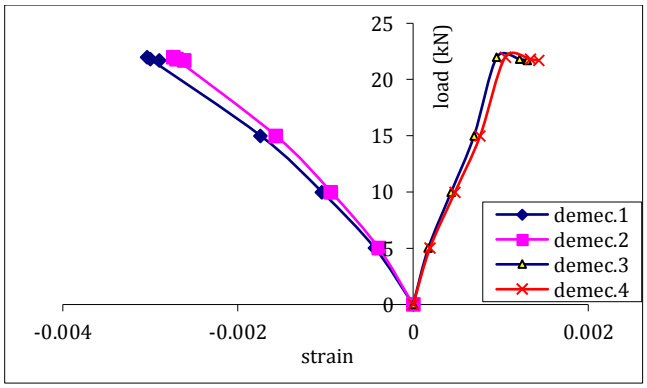

Fig. 19. Load-Strain curve of S4.

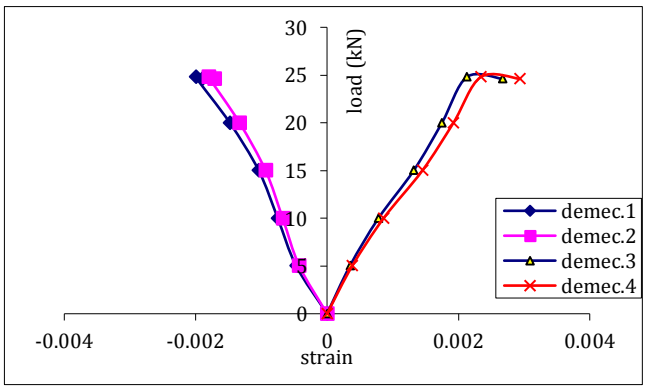

Fig. 20. Load-Strain curve of S5.

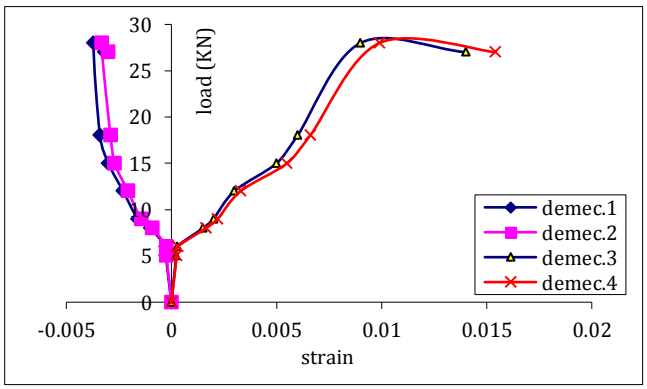

Fig. 21. Load-Strain curve of S6.

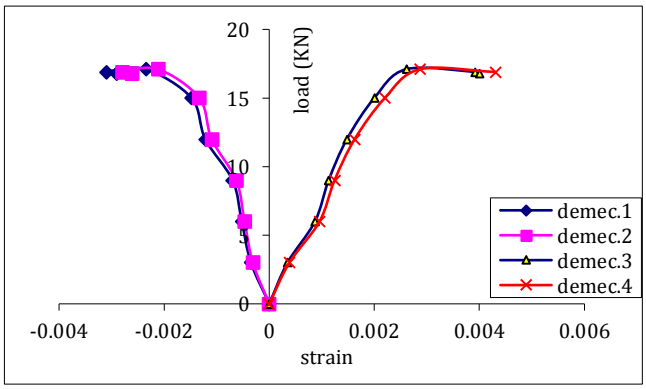

Fig. 22. Load-Strain curve of S7.

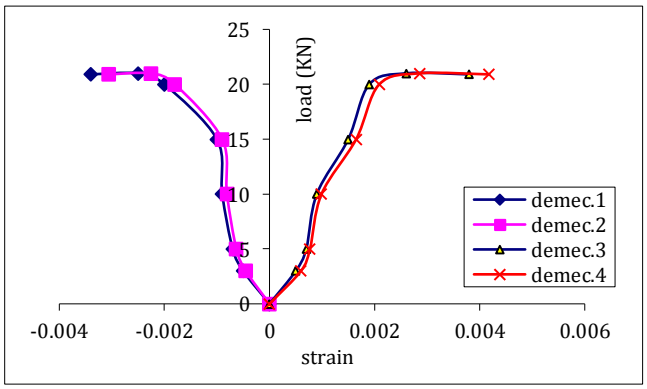

Fig. 23. Load-Strain curve of S8.

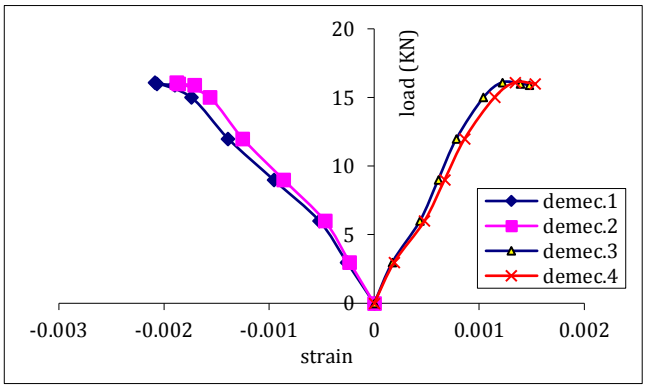

Fig. 24. Load-Strain curve of S9.

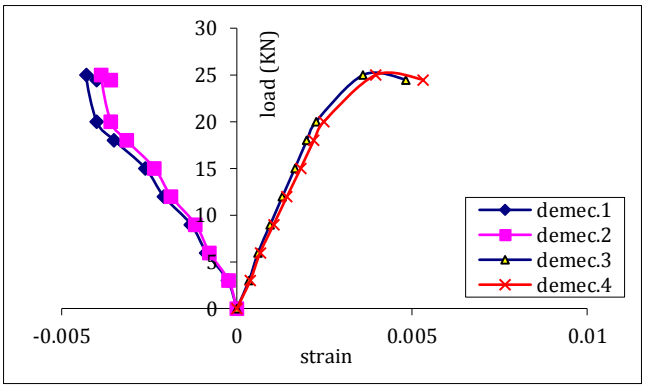

Fig. 25. Load-Strain curve of S10.

3.5. Cracking pattern and mode of failure

3.5.1. Control specimen

Fig. 26 shows the tensile crack, compressive crack and side views of crack patterns of all the tested slabs.

For designation A, flexural crack developed near the mid-span of the specimens of this designation at load of approximately 10 and 15 kN, for slab S1 and S2 respectively. Upon increasing the load, the cracks propagated rapidly upwards and increased in number along the span.

The length and width of the cracks increased with the increase of the applied load. Moreover, diagonal or inclined cracks developed at both ends of the specimen. Failure of the control specimens occurred due to flexure and crushing of the concrete surface at load of 19 kN for S1 and 23.3 kN for S2 as shown in Fig. 26.

3.5.2. Specimens incorporating ferrocement forms reinforced with expanded steel mesh

For designation (B) slabs S3 and S4, it is interesting to note that vertical flexural crack started to develop close to the centre of the span. As the load increased, more cracks started to develop in S3 and S4 and the crack at mid-span started to propagate vertically towards the top surface of the specimen. The crack widths were much less than those of designation A control, this could be attributed to the effect of No. of steel meshes in controlling the crack width. Failure of this type of specimens occurred due to flexural failure as shown in Fig. 26.

3.5.3. Specimens incorporating ferrocement forms reinforced with welded steel mesh

For designation (C) slabs S5 and S6, which reinforced with two and four layers of welded galvanized steel mesh size respectively, it is interesting to note that vertical flexural crack started to develop close to the centre of the span. As the load increased, more cracks started to develop in S5 and S6 and the crack at mid-span started to propagate vertically towards the top surface of the specimen. The crack widths were much less than those of designations A and B. This could be attributed to the effect of No. of steel meshes in controlling the crack width. The flexural crack developed near the mid-span of the specimens of this designation at load of approximately 15 kN and 18 kN for slabs S5 and S6 respectively. With increasing the load, the cracks propagated vertically and new flexural cracks were developed rapidly. As the specimens approached their failure load, the crack started to propagate wider. Failure of this type of specimens occurred due to flexural failure. There is no spalling of concrete cover this is predominant as shown in Fig. 26.

3.5.4. Specimens incorporating ferrocement forms reinforced with fiberglass steel mesh

For designation (D) slabs S7 and S8 which reinforced with one and two layers of fibre glass meshes respectively. It is interesting to note that vertical flexural crack for this type of specimens stared at mid-span and propagated vertically towards the top side of the beam and increased in number along the span. The rate of crack propagation was less than that for the control specimen. Although the crack width was not measured in the test, the visual crack width was less than that of the control specimen. Failure of this type of specimens occurred after crack. Flexural crack developed near the mid-span of the specimens of this designation at load of approximately 15 kN for slabs S7 and S8. Flexural ultimate loads for slabs S7 and S8 reached 17.1 and 21 kN respectively. Fig. 26 shows the cracking pattern of all the tested U shape slabs.

3.5.5. Specimens incorporating ferrocement forms reinforced with fiberglass steel mesh

For designation (D) slabs S7 and S8 which reinforced with one and two layers of fibre glass meshes respectively. It is interesting to note that vertical flexural crack for this type of specimens stared at mid-span and propagated vertically towards the top side of the beam and increased in number along the span. The rate of crack propagation was less than that for the control specimen. Although the crack width was not measured in the test, the visual crack width was less than that of the control specimen. Failure of this type of specimens occurred after crack. Flexural crack developed near the mid-span of the specimens of this designation at load of approximately 15 kN for slabs S7 and S8. Flexural ultimate loads for slabs S7 and S8 reached 17.1 and 21 kN respectively. Fig. 26 shows the cracking pattern of all the tested U shape slabs.

Crack pattern of S1

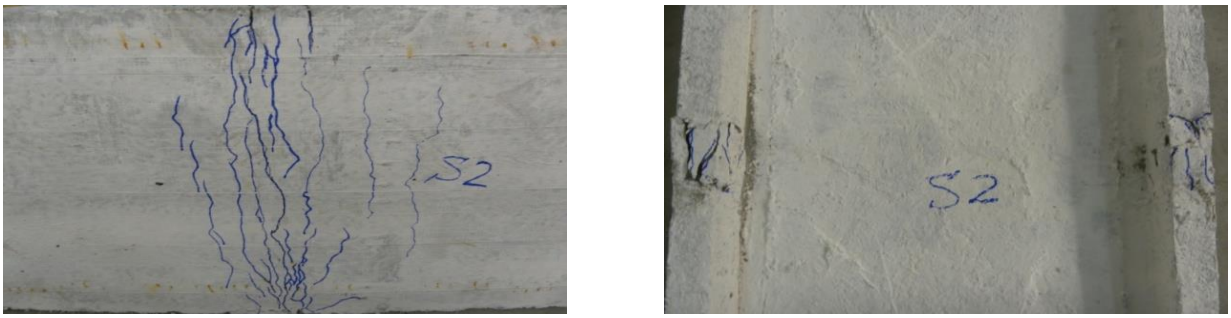

Crack pattern of S2

Crack pattern of S3

Crack pattern of S4

Crack pattern of S5

Crack pattern of S6

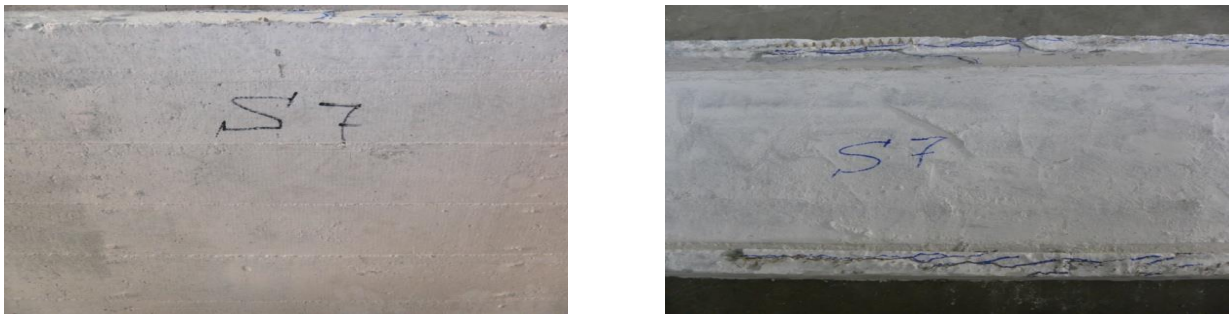

Crack pattern of S7

Crack pattern of S8

Crack pattern of S9

Crack pattern of S10

Fig. 26. Crack patterns of all tested slabs.

3.6. Effect of the test parameters

The effect of the test parameter is investigated from the experimental results of the test specimens and is discussed in the following sections. The effects of these parameters were studied on the structural responses of the test U shape slabs in terms of first crack load, service load, and failure load, mode of failure, ductility ratio, and energy absorption.

The load-deflection relationship for the control specimens was linear up to a load of approximately 15 kN approximately, when the first crack was observed, after which the relation became nonlinearly. Beyond load of about 17 kN the mid-span deflection increased with much higher rate indicating yielding of the steel reinforcement. At failure, the mid-span deflection reached 35 mm.

3.6.1. Effect of the existence of synthetic fibres in the mortar mix

The effect of the existence of the synthetic fibres in the mix of the ferrocement mortar on the behaviour of the test specimens is studied by comparing the results of the same specimens containing the fibres in the mix with the corresponding ones without the fibres for series A. and for all groups with others.

The behaviour of the specimens without synthetic fibres was considered as the base for this comparison, the existence of the synthetic fibres in the mortar mix resulted in an increase in the first crack load, serviceability load, ultimate load, and energy absorption. However, it resulted in a decrease in the ductility ratio. Fig. 15 shows the comparison between the load deflection curves for all test specimens.

The existence of the synthetic fibres resulted in retarding the occurrence of the first crack and better crack distribution in the ferrocement U-shaped slabs. This led to a higher stiffness of the test specimen and consequently less deflection at the corresponding load levels as shown in Figs. 11-14. The figures show that the specimens with fibre had a higher deflection at failure as a result of the attained higher ultimate load. However, the ratio of the deflection at ultimate load to that at the first cracking load was lower for the specimens with fibres in comparison to those without fibres which lead to the observed reduction of the ductility ratio as defined in this research.

3.6.2. Effect of the type of the mesh inside the U shape slabs

The effect of reinforcing steel mesh type is studied by comparing the results of groups reinforced with expanded wire mesh with that reinforced with welded steel mesh and fibreglass mesh. The behaviour of expanded wire mesh group was considered as the base for comparison for both single and double layers.

Samples reinforced with welded wire mesh achieved higher first crack load, ultimate load, serviceability load and energy absorption with respect to steel bars and the number of steel mesh.

It is worth mentioning that the ductility of slabs reinforced with expanded wire mesh is higher than that of beams reinforced with welded wire mesh. This is expected since the specimens reinforced with expanded steel mesh had slightly higher volume fraction, 0.04% and 0.231%. However, the proof stress for the expanded steel mesh was much lower than that for the welded wire mesh, 199 N/mm^2 as compared to 400N/mm^2.

3.6.3. Effect of the number of reinforcing steel mesh layers

The effect of the number of reinforcing steel mesh layers is investigated by comparing the results of groups reinforced with single and double layers for both steel mesh types investigated in this research. Doubling the steel mesh layers at the bottom of the specimens resulted in a higher first crack load, serviceability load, ultimate load, and energy absorption. However, the maximum deflection at ultimate load decreased as a result of increasing the specimen's stiffness also the ductility ratio decreased due to the increase of the volume fraction.

The enhancement in mechanical properties due to increasing the number of steel mesh layers for welded wire mesh was much higher than that of expanded wire mesh for the first crack load, ultimate load, and serviceability load and energy absorption. However, the enhancement in reduction in the ductility ratio was almost the same for both types of steel mesh.

4. Conclusions

The results also demonstrated that the presence of fibres in the mix improved the slab's overall performance. Within the scope, parameters, experimental investigation considered in this research and based on the test results and observations of the experimental investigation; the following conclusions and recommendations may be drawn as follows:

- Employing welded galvanized steel mesh gave the highest results compared to all tested U shape tested slabs.
- Using polypropylene fibres in mortar mix increase in the first crack load, serviceability load, ultimate load, and energy absorption, higher stiffness However, it resulted in a decrease in the ductility ratio, less deflection at the corresponding load levels.
- Welded galvanized wire mesh achieved higher first crack load, serviceability load, ultimate load and energy absorption in comparison to reinforce with expanded and glass fibre meshes..
- Using (two-four) layers of welded galvanized steel mesh in reinforcing ferrocement U shaped slabs, improve the energy absorption than obtained when using skeletal steel bars.
- Using U-shaped welded steel mesh with mild steel bars in reinforcing ferrocement slabs higher energy absorption than of using mild steel bars only. However the U-shaped showed less ductility ratio.
- Using four steel bars with one layer expanded metal mesh improve ductility ratio and energy absorption compared with using two-layer expanded metal mesh only.

- Increasing the number of the steel mesh layers in the ferrocement forms increases the first crack load, service load, ultimate load, and energy absorption decreases the ductility ratio of the U shaped slab.
- Using welded steel wire mesh reinforcement decreased the ductility ratio compared to that reinforced with glass fibre mesh and expanded steel mesh.
- The ductility ratio reduced. The percentage of reduction depends on the type and number of steel mesh layers in the ferrocement U shaped forms.

REFERENCES

Abdel Tawab A (2006). Development of Permanent Formwork for Beams Using Ferrocement Laminates. *Ph.D thesis*, Menoufia University, Shebin El-Kom, Egypt.

Abdul Kadir MR, Jaafar MSH (1993). Ferrocement in situ permanent formwork. *Journal of Ferrocement*, 23(2), 125-133.

Abdul Kadir MR, Abdul Samad AA, Che Muda Z, Ali AAA (1997). Flexural Behavior of Composite Beam with ferrocement Permanent Formwork. *Journal of Ferrocement*, 27, 209 - 214.

ACI 549-1R-88 (1998). Guide for the Design, Construction, and Repair of Ferrocement, Manual of Concrete Practice. American Concrete Institute, Farmington Hill, Michigan, USA.

Ayoub STAE (2005). Flexural Behavior of High Strength Concrete Beams Reinforced with Advanced Composite Materials. *M.Sc thesis*, Menoufia University, Shebin El-Kom, Egypt.

Channi AS (2009). Effect of Percentage of Reinforcement on Beams Retrofitted with Ferrocement Jacketing. *M.Sc thesis,* Thapar University, Patiala, India.

El-Halfawy EMAF (2003). Flexural Behavior of Ferrocement Deck Bridges. *M.Sc thesis*, Menoufia University, Shebin El-Kom, Egypt.

ElMohimen HMRA (2005). Structural Behaviour of Ribbed Ferrocement Plate. *B.Sc thesis*, Menoufia University, Shebin El-Kom, Egypt.

El-Sakhawy YME (2007). Structural Behaviour of Ferrocement Roof Elements. *M.Sc thesis*, Menoufia University, Shebin El-Kom, Egypt.

Fahmy EH, Shaheen YBI (1991). Strengthening and repairing of reinforced concrete tanks. *Fourth Arab Structural Engineering Conference*, United Arab Emirates, 18-21.

Fahmy EH, Shaheen YBI, El-Dessouki WM (1995). Application of ferrocement for construction of radial gates. *Journal of Ferrocement,* 25(2), 115-121.

Fahmy EH, Shaheen YBI, Korany YS (1997a). Repairing reinforced concrete beams by ferrocement. *Journal of Ferrocement*, 27(1), 19-32.

Fahmy EH, Shaheen YBI, Korany YS (1997b). Use of ferrocement laminates for repairing reinforced concrete slabs. *Journal of Ferrocement*, 27(3), 219-232.

Fahmy EH, Shaheen YBI, Korany YS (1999). Repairing reinforced concrete columns using ferrocement laminates. *Journal of Ferrocement*, 29(2), 115-124.

Fahmy EH, Shaheen YBI, Abou Zeid MN (2004). Development of ferrocement panels for floor and wall construction. *5th Structural Specialty Conference of the Canadian Society for Civil Engineering*, Canada.

Housing and Building Research Center (HBRC) (2001). The Egyptian Code for Design and Construction of Concrete Structures, Cairo, Egypt.

Mansur MA, Paramasivam P (1990). Ferrocement short columns under axial and eccentric compression. *ACI Structural Journal*, 87(5), 523-529.

Mays GC, Barnes RA (1995). Ferrocement permanent formwork as protection to reinforced concrete. *Journal of Ferrocem*ent, 25(4), 331-345.

Naaman AE, Shah SP (1971). Tensile tests of ferrocement. *ACI Journal*, 68(9), 693-698.

Rajagoplan K, Parameswaran VS (1975). Analysis of ferrocement beams. *Journal of Structural Engineering*, 2(4), 155-164.

Ramesht MH, Vickridge I (1996). A computer program for the analysis of ferrocement in flexure. *Journal of Ferrocement*, 26(1), 21- 31.

Rao PK, Rao VJ (1987). Development and application of composite precast ferrocement and concrete roofing/flooring system. *Proceedings of the First International Conference on Structural Science and Engineering*, India.

Rosenthal I, Bljuger F (1985). Bending behavior of ferrocement – reinforced concrete composite. *Journal of Ferrocement*, 15(1), 15-24.

Sandowicz M, Grabowski J (1985). Application of ferrocement channel elements to housing. *Proceedings of the Second International Symposium on Ferrocement,* International Ferrocement Information Center, Bangkok. 493- 505.

Shaheen YBI, Eltaly B, Henish A (2014). Experimental and FE simulations of ferrocement domes reinforced with composite materials. *Concrete Research Letters*, 5(4), 837-887.

Shaheen YBI, Mahmoud AM, Refat HM (2016). Structural performance of ribbed ferrocement plates reinforced with composite materials. *Structural and Engineering Mechanics*, 60(4), 567-594.

Singh G, Bennett EW, Fakhri NA (1988). Influence of reinforcement on fatigue of ferrocement. *The International Journal of Cement Composites and Lightweight Concrete*, 8(3), 151-164.

Sutherland WM (1972). Ferrocement Boats: Service Experience in New Zealand. *FAO Seminar on the Design and Construction of Ferrocement Fishing Vessels*, Wellington, 14 (Also, Fishing News, West Byfleet, Surrey).

Swamy RN, Abboud MI (1988). Application of ferrocement concept to low cost lightweight concrete sandwich panels. *Journal of Ferrocement*, 18(3), 285-292.

Tomar A (2006). Retrofitting of Shear Deficient RC Beams using Ferrocement Laminates. *M.Sc thesis,* Thapar Institute of Engineering and Technology (Deemed University), Patiala, India.

Wrigley RG (2001). Permanent Formwork in Construction. Construction Industry Research & Information Association (CIRIA), London.

Challenge Journal of Concrete Research Letters

Evaluation of initial setting time due to superplasticizers

Abhishek Singh [a,*], Shobha Ram [a], Alok Verma [b]

[a] *Department of Civil Engineering, Gautam Buddha University, Uttar Pradesh, India*
[b] *Department of Civil Engineering, Delhi Technological University, Delhi, India*

ABSTRACT

This paper shows how polycarboxylate based superplasticizer affects the initial setting time of cement paste. Three superplasticizers are used in this study with different properties and aiming to determine the delay in initial setting time due to superplasticizer. Initial setting time is calculated as per IS: 4031-PART 5-1988 with different SP dosages (0.5%, 0.75%, 1.0% and 1.5% of weight of cement). Superplasticizer is an admixture which reduces the water-cement ratio or increase the workability at the same water content. This paper deals with the evaluation of initial setting time due to superplasticizers.

ARTICLE INFO

Article history:
Received 11 April 2017
Revised 9 June 2017
Accepted 19 June 2017

Keywords:
Polycarboxylate
Superplasticizers
Initial setting time
Dosages

1. Introduction

Setting time of cement paste is characterized as the time required for the move of cement paste from fluid phase to solid phase. It is vital to recognize this stage as this stage helps in setting and transporting cement paste. Superplasticizer (S.P) is a type of water reducers, however, the difference between superplasticizer and water reducer is that superplasticizer will significantly reduce the water required for concrete mixing. Generally, there are four main categories of superplasticizer: sulfonated melamine formaldehyde condensates, sulfonated naphthalene formaldehyde condensates, modified lignosulfonates and others such as sulfonic-acid esters and carbohydrate esters (Alsadey, 2015). In this study, polycarboxylate ether based superplasticizer is used. It consists of a carboxylic ether polymer with long side chains. Toward the start of the mixing process it starts an indistinguishable electrostatic scattering mechanism from the customary superplasticizers, however the side chains connected to the polymer spine produces a steric hinderance which enormously balances out the concrete particles capacity to separate and disperse. Steric hinderance gives a physical obstruction (nearby the electrostatic boundary) between the cement grains. With this procedure, flowable paste with incredibly decreased water content is obtained.

Superplasticizers are frequently used in order to improve the workability of mortar and concrete mixes for demanding applications. The addition of superplasticizers aims at two objectives: first, the addition of superplasticizers allows controlling the flow properties, which are of major importance for the design of self-compacting concretes, and second, superplasticizers allow the reduction of the water to cement ratio while maintaining workability in order to reach high strength and durability. The cement–water system is highly sensitive to the addition of superplasticizers. Small amounts of superplasticizers enhance the workability properties efficiently, but are often associated with strong, undesired retardation phenomena of the setting of the cement paste (Zingg et al., 2009).

Impact of superplasticizer on compressive quality have been explored by Papo and Piani (2004), Sakai et al. (2006), Shi et al. (2009), and Kadri et al. (2009). Setting and hardening of cement relies on upon numerous elements, for example, water-bond proportion, bond quality, nature of solid material, quality control amid generation of cement and so forth (Mahmoud et al., 2010; Sukumar and Silva, 2016). SP cause better scattering and effect of superplasticizers on porosity have been seen (Memon et al., 2002; Liao et al., 2004; Gastaldini et al., 2009).

* *Corresponding author*. Tel.: +91-999-9471478 ; E-mail address: abhishek180694@gmail.com (A. Singh)
ISSN: 2548-0928 / DOI: https://doi.org/10.20528/cjcrl.2017.02.003

Adsorption, fluidity and hydration property have been studied and it has been reported that use of superplasticizers improves these properties (Yoshiokaa et al., 2002; Kong et al., 2006; Plank and Hirsch, 2007; Mikanovic and Jolicoeur, 2008; Pei et al., 2008). Durability, pore size distribution and rheological properties have been investigated and beneficial effect of superplasticizer have been reported (Caszewski and Szwabowski, 2004; Houst et al., 2008; Roziere et al., 2009; Li et al., 2009; Felekoglu et al., 2009).

Effect of Superplasticizers on setting time and has been compared with other superplasticizer having different base (Palacios et al., 2009; Zhang et al., 2010). In practice, the initial set indicates the loss of workability and the beginning of the stiffening of the paste.

2. Experimental Programme

It was intended to observe the effect of superplasticizer on setting of cement pastes when mixed in different dosages and to compare the performances of various superplasticizers. The experimental programme included the use of three types of superplasticizers with different properties.

In present investigations, four superplasticizer dosages (0.5%. 0.75%, 1%, 2% of weight of cement) are provided in cement and cement paste is prepared with the desired consistency. Abbreviations of some cement mix designations are explained below in Table 1. Superplasticizer properties are given below in Table 2 respectively. Vicat apparatus was used as per standard procedure with different dosages of the three superplasticizers and their effect on initial setting time has been seen as per IS: 4031-PART 5-1988 respectively. Penetration readings were taken after every 5 minutes to assess change in rheological properties.

Table 1. Explanation of mortar mix designations.

Typical Mix Designation	Explanation
C1-0%	Cement Type 1 SP Dosage 0%
C2-0%	Cement Type 2 SP Dosage 0%
C3-0%	Cement Type 2 SP Dosage 0%

Table 2. Characteristics of superplasticizer.

Type	Solid Content	Specific Gravity	pH	Grade
Type-1	40%	1.1	5	Neutral
Type-2	60%	1.58	8	Alkaline
Type-3	70%	1.05	>6	Alkaline

3. Results and Discussion

Cement pastes with different dosages of Superplasticizers were prepared and penetration of needle after every five minutes is noted which is described in Tables 4-6 respectively included graphs with trendline equations.

It has been investigated that there is a delay in initial setting time with increase in superplasticizer dosage. Consistency of the cement paste decreases with increase of superplasticizer as shown in Table 3.

Table 3. Consistency of superplasticizers.

SP Type	Dosage	Consistency
Type -1	0.5%	29.5%
	0.75%	28.55%
	1.0%	27.7%
	1.5%	26.5%
Type -2	0.5%	28.75%
	0.75%	28.12%
	1.0%	27.4%
	1.5%	26.65%
Type -3	0.5%	25.75%
	0.75%	24.5%
	1.0%	23.5%
	1.5%	22.0%

Table 4. Penetration at every 5 minutes for Type-1 SP.

Time (minutes)	SP Dosage (%)			
	0.5%	0.75%	1.0%	1.5%
0	0	0	0	0
5	0	0	0	0
10	0	0	0	0
15	0.5	0	0	0
20	1.5	1.0	0	0
25	2.0	1.5	0	0
30	2.5	2.0	0.5	0
35	3.0	2.5	1.0	0
40	4.0	3.0	1.5	0
45	4.5	3.5	2.0	0.5
50	5.50	4.0	2.5	1.0
55		5.0	3.0	1.5
60		6.0	3.5	1.8
65			4.5	2.0
70			4.8	2.5
75			5.5	3.0
80				3.5
85				4.0
90				4.5
95				6.0
IST (minutes)	50	60	75	95

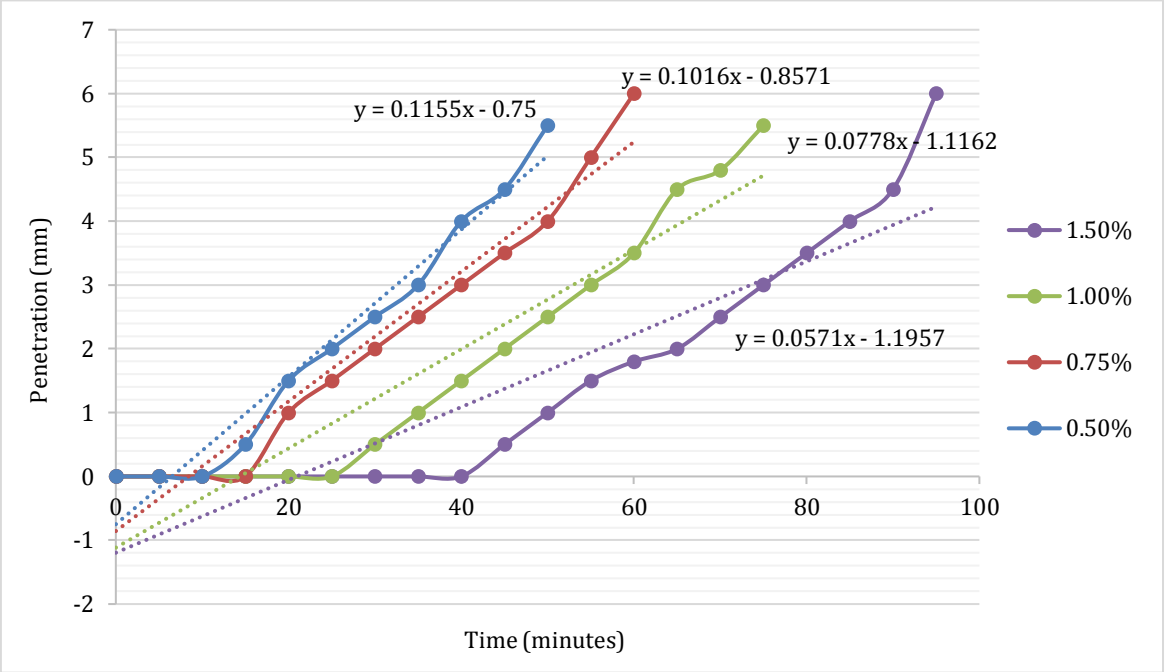

Fig. 1. Penetration for Type-1 superplasticizer.

Table 5. Penetration at every 5 minutes for Type-2 SP.

Time (minutes)	SP Dosage (%)			
	0.5%	0.75%	1.0%	1.5%
0	0	0	0	0
5	0	0	0	0
10	0	0	0	0
15	2.0	0	0	0
20	3.0	0.5	0	0
25	3.5	1.0	0	0
30	4.0	1.5	0.5	0
35	4.5	2.5	1.0	0
40	5.0	3.0	1.5	0.5
45	5.5	4.5	2.5	1.0
50		4.8	3.0	1.0
55		5.5	3.5	1.5
60			4.0	2.0
65			4.0	2.5
70			5.5	3.5
75				4.0
80				5.0
85				5.5
IST (minutes)	45	55	70	85

Table 6. Penetration at every 5 minutes for Type-3 SP.

Time (minutes)	SP Dosage (%)			
	0.5%	0.75%	1.0%	1.5%
0	0	0	0	0
5	0	0	0	0
10	0.5	0	0	0
15	1.5	0	0	0
20	2.5	0.5	0	0
25	3.0	1.5	0	0
30	3.5	2.5	0	0
35	4.5	3.5	0.5	0
40	5.5	4.0	1.5	0.5
45		4.5	2.0	1.0
50		6.0	2.5	1.5
55			3.5	2.5
60			4.5	3.0
65			5.5	3.5
70				4.5
75				5.5
IST (minutes)	40	50	65	75

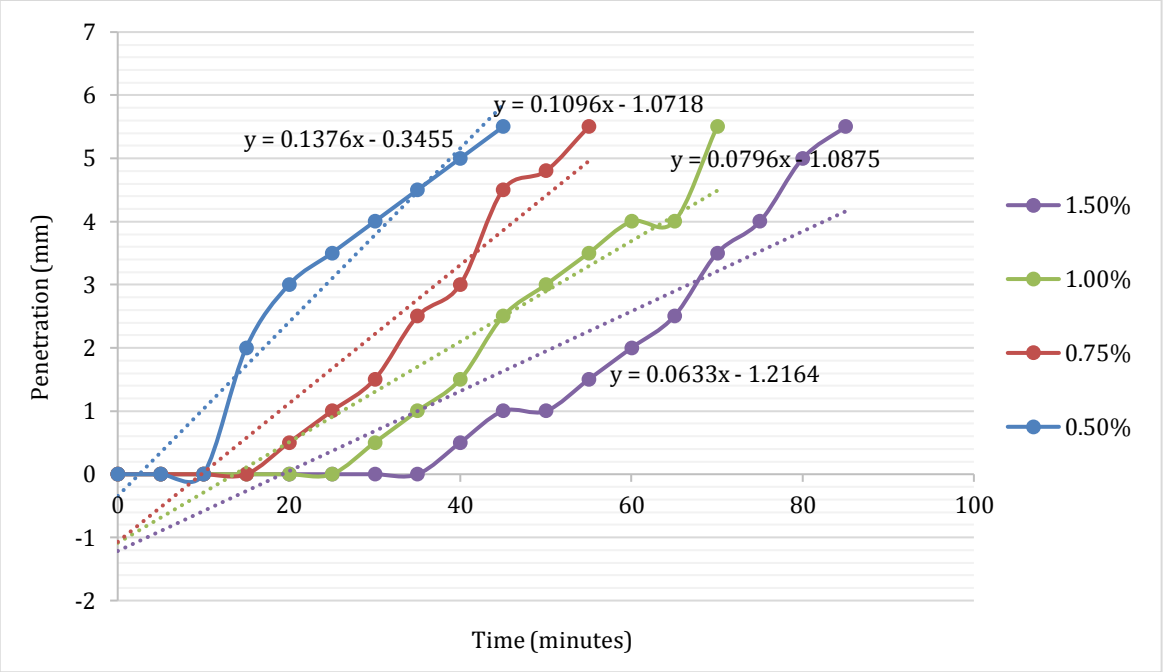

Fig. 2. Penetration for Type-2 superplasticizer.

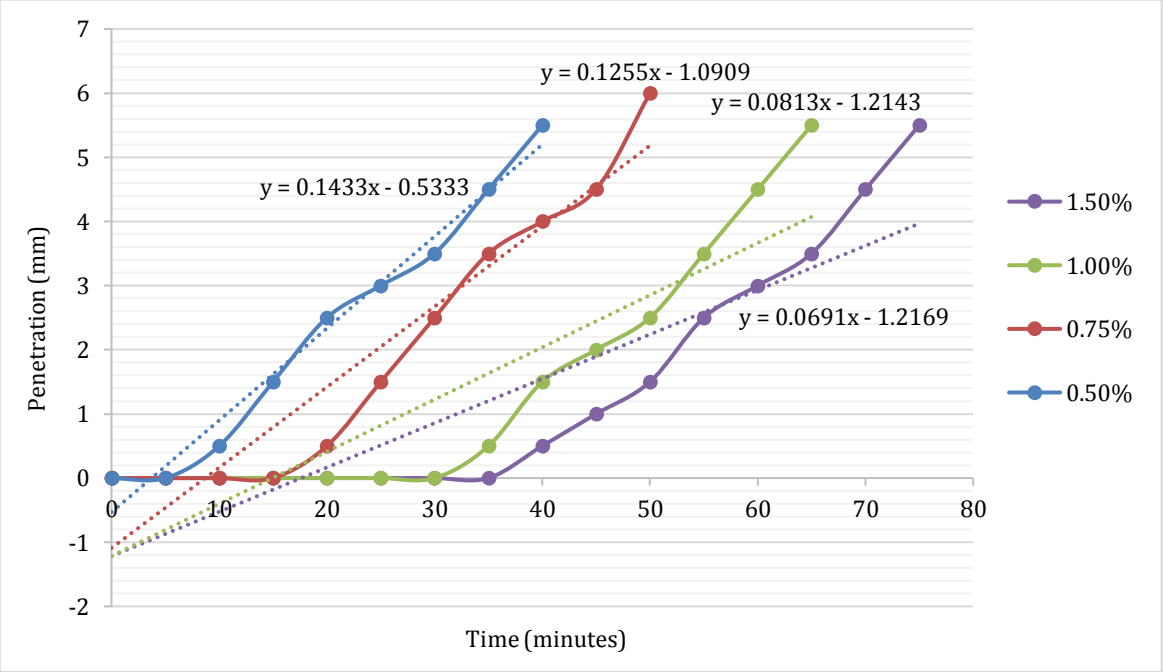

Fig. 3. Penetration for Type-3 superplasticizer.

From Fig. 1, it is seen that there is significant increase of 20% in initial setting time when dosage increased to 0.75% from 0.5%. However increase of nearly 26% is experienced when dosage increased to 1% from 0.75% and from 1% to 1.5%. Increase of 50% in initial setting time when SP dosage increased directly to 1% from SP dosage 0.5% of weight of cement.

For type-2 superplasticizer it can be seen that there is an increase of 22% in initial setting time when dosage increased to 0.75% from 0.5%, however increase of nearly 15% increase is experienced when dosage increased to 1% from 0.75% and from 1% to 1.5%. Increase of 55% in initial setting time is there when SP dosage increased directly to 1% from SP dosage of 0.5% of weight of cement.

It has been investigate that in type-3 superplasticizer there is increase of 25% in initial setting time when dosage increased to 0.75% from 0.5%, however increase of nearly 20% increase is experienced when dosage increased to 1% from 0.75% and from 1% to 1.5%. Increase of approximately 62% in initial setting time when SP dosage increased directly to 1% from SP dosage 0.5% of weight of cement.

4. Conclusions

Since the initial setting time indicates the loss of workability to such an extent that the paste is no longer workable, the initial setting time is determined by the penetration depth test of the cement pastes via vicat apparatus. A superplasticizer reduces the required water cement ratio but at the same time delays the setting time of cement paste.

- It is seen that type-1 superplasticizer reduces up to 30% water whereas type-2 Superplasticizer reduces 40% water and type-3 reduces 45% water. This indicates that initial setting time of cement can be modified and regulated with the use of superplasticizers.
- Since the use of SP delays setting, the timing and effect of redosages of SP can be worked out, as indicated by zeros in table 4, 5 and 6 respectively.
- Effectiveness of various SPs could be compared by examining delay of initial setting time with percentage of dosages, as provided in last rows of table 4, 5 and 6 respectively.
- Indicative equations are shown for different curves in Figs. 1-3 which may be used to provide data about consistency before initial setting is complete.

References

Alsadey S (2015). Effect of superplasticizer on fresh and hardened properties of concrete. *Journal of Agricultural Science and Engineering,* 1(2), 70-74.

Caszewski JC, Szwabowski J (2004). Influence of superplasticizers on rheological behaviour of fresh cement mortars. *Cement and Concrete Research,* 34, 235–248.

Felekoglu B, Turkel S, Kalyoncu H (2009). Optimization of fineness to maximize the strength activity of high-calcium ground fly ash – Portland cement composites. *Construction and Building Materials,* 23, 2053–2061.

Gastaldini ALG, Isaia GC, Hoppe TF, Missau F, Saciloto AP (2009). Influence of the use of rice husk ash on the electrical resistivity of concrete: A technical and economic feasibility study. *Construction and Building Materials,* 23, 3411–3419.

Houst YF, Bowen P, Perche F, Kauppi A, Borgett P, Galmiche L, Le Meins J-F, Lafuma F, Flatt RJ, Schober I, Banfill PFG, Swift DS, Myrvold BO, Petersen BG, Reknes K (2008). Design and function of novel superplasticizers for more durable high performance concrete (superplast project). *Cement and Concrete Research,* 38, 1197–1209.

Kadri E-H, Aggoun S, De Schutter G (2009). Interaction between C3A, silica fume and naphthalene sulphonate superplasticiser in high performance concrete. *Construction and Building Materials,* 23, 3124–3128.

Kong HJ, Bike SG, Li VC (2006). Effects of a strong polyelectrolyte on the rheological properties of concentrated cementitious suspensions. *Cement and Concrete Research,* 36, 851–857.

Li G, Xiong G, Lu Y, Yin Y (2009). The physical and chemical effects of long-term sulphuric acid exposure on hybrid modified cement mortar. *Cement & Concrete Composites,* 31, 325–330.

Liao K-Y, Chang P-K, Peng Y-N, Yang C-C (2004). A study on characteristics of interfacial transition zone in concrete. *Cement and Concrete Research,* 34, 977–989.

Mahmoud AAM, Shehab MSH, El-Dieb AS (2010). Concrete mixtures incorporating synthesized sulfonated acetophenone–formaldehyde resin as superplasticizer. *Cement & Concrete Composites,* 32, 392–397.

Memon AH, Radin SS, Zainc MFM Trottier J-F (2002). Effects of mineral and chemical admixtures on high-strength concrete in seawater. *Cement and Concrete Research,* 32, 373–377.

Mikanovic N, Jolicoeur C (2008). Influence of superplasticizers on the rheology and stability of limestone and cement pastes. *Cement and Concrete Research,* 38, 907–919.

Palacios M, Houst YF, Bowen P, Puertas F (2009). Adsorption of superplasticizer admixtures on alkali-activated slag pastes. *Cement and Concrete Research,* 39, 670–677.

Papo A, Piani L (2004). Effect of various superplasticizers on the rheological properties of Portland cement pastes. *Cement and Concrete Research,* 34, 2097–2101.

Pei M, Wang Z, Li W, Zhang J, Pan Q, Qin X (2008). The properties of cementitious materials superplasticized with two superplasticizers based on aminosulfonate–phenol–formaldehyde. *Construction and Building Materials,* 22, 2382–2385.

Plank J, Hirsch C (2007). Impact of zeta potential of early cement hydration phases on superplasticizer adsorption. *Cement and Concrete Research,* 37, 537–542.

Roziere E, Loukili A, El Hachem R, Grondin F (2009). Durability of concrete exposed to leaching and external sulphate attacks. *Cement and Concrete Research,* 39, 1188–1198.

Sakai E, Kasuga T, Sugiyama T, Asaga K, Daimon M (2006). Influence of superplasticizers on the hydration of cement and the pore structure of hardened cement. *Cement and Concrete Research,* 36, 2049–2053.

Shi H-S, Xu B-W, Zhou X-C (2009). Influence of mineral admixtures on compressive strength, gas permeability and carbonation of high performance concrete. *Construction and Building Materials,* 23, 1980–1985.

Sukumar B, Silva J (2016). Effect of polymeric admixtures on self-compacting concrete. *International Journal of Innovative Research in Science, Engineering and Technology,* 5(1), 660-665.

Yoshiokaa K, Tazawa E, Kawai K, Enohata T (2002). Adsorption characteristics of superplasticizers on cement component minerals. *Cement and Concrete Research,* 32, 1507–1513.

Zhang M-H, Sisomphon K, Ng TS, Sun DJ (2010). Effect of superplasticizers on workability retention and initial setting time of cement pastes. *Construction and Building Materials,* 24, 1700–1707.

Zingg A, Winnefeld F, Holzer L, Pakusch J, Becker S, Figi R, Gauckler L (2009). Interaction of polycarboxylate-based superplasticizers with cements containing different C3A amounts. *Cement & Concrete Composites,* 31, 153–162.